

THESIS

METABOLIC ENGINEERING INTERVENTIONS FOR SUSTAINABLE 2,3-BUTANEDIOL
PRODUCTION IN GAS FERMENTING CLOSTRIDIUM AUTOETHANOGENUM

Submitted by

Parsa Ghadermazi

Department of Chemical and Biological Engineering

In partial fulfillment of the requirements

For the Degree of Master of Science

Colorado State University

Fort Collins, Colorado

Spring 2023

Master's Committee:

Advisor: Siu Hung Chan

Kelly Wrighton
Brad Reisfeld

Copyright by Parsa Ghadermazi 2023

All Rights Reserved

ABSTRACT

METABOLIC ENGINEERING INTERVENTIONS FOR SUSTAINABLE 2,3-BUTANEDIOL PRODUCTION IN GAS FERMENTING CLOSTRIDIUM AUTOETHANOGENUM

Gas fermentation provides a promising platform to turn low-cost and readily available single-carbon waste gases into commodity chemicals such as 2,3-butanediol. *Clostridium autoethanogenum* is usually used as a robust and flexible chassis for gas fermentation. Here, we leveraged on constraints-based stoichiometric modeling and kinetic ensemble modeling of the *C. autoethanogenum* metabolic network to provide a systematic *in silico* analysis of metabolic engineering interventions for 2,3-butanediol overproduction and low carbon substrate loss in dissipated CO₂. Our analysis allowed us to identify and to assess comparatively the expected performances for a wide range of single, double, and triple interventions. Our analysis managed to individuate bottleneck reactions in relevant metabolic pathways when suggesting intervening strategies. Besides recapitulating intuitive and/or previously attempted genetic modifications, our analysis neatly outlined that the interventions - at least partially - impinging on by-products branching from acetyl-CoA and pyruvate (acetate, ethanol, amino acids) offer valuable alternatives to the interventions focusing directly on the specific branch from pyruvate to 2,3-butanediol.

ACKNOWLEDGEMENTS

I deeply appreciate the invaluable guidance, great support, and patience that Dr. Siu Hung Joshua Chan, my supervisor, has provided throughout my academic research. His vast knowledge and experience have been a constant source of motivation for me. I am also grateful to my collaborators, Angela Re and Luca Ricci, for their assistance throughout the entire project. Additionally, I would like to express my thanks to my committee members, Dr. Kelly Wrighton and Dr. Brad Reisfeld, for their insightful comments. Finally, I am thankful to my family for their understanding and encouragement, without which I could not have completed my master's program.

TABLE OF CONTENTS

ABSTRACT.....	ii
ACKNOWLEDGEMENTS	iii
Introduction.....	1
Results and Discussion	7
Model validation.....	7
Analysis of the effect of H ₂ on 2,3-butanediol and CO ₂ production.....	10
Prediction of genetic manipulations leading to 2,3-butanediol overproduction.....	11
PFOR up-regulation predicted to be the most effective single intervention.....	16
Overexpression of both PFOR and ACLS predicted as the most effective double intervention.....	20
Overexpression of ACLDC on top of PFOR and ACLS predicted to be the most effective triple intervention.....	28
Materials and Methods.....	37
Genome-scale stoichiometric metabolic model.....	37
Flux through the network with zero exchanges.....	38
Flux through ATP hydrolysis reaction with zero uptakes	38
Condition-specific model validation.....	38
Relationship between gas feeding and CO ₂ production.....	39
Prediction of interventions enhancing 2,3-butanediol production.....	39
Simulations using the kinetic model of <i>C. autoethanogenum</i>	40
References.....	42
Appendix.....	47
Supplementary File 1.....	47
Supplementary File 2.....	47
Supplementary Figure 1.....	47
Supplementary Figure 2.....	48

Introduction¹

Rethinking complex value chains is a key priority to achieve a modern, low-carbon, resource- and energy-efficient economy. Sustainable and carbon circular economy models are being developed to offer functionalities analogous or superior to traditional commodities with potentially lower environmental impacts, but they currently represent a very small share of the market. One component of the technological innovations necessary to attain carbon recycling can be the application of bioprocesses enabling conversion of C₁-based industrial waste gas streams into commodity chemicals (1-2). Carbon monoxide (CO) is a major by-product of the incomplete combustion of carbon-based fuels—including coal, oil, natural gas and wood. Furthermore, CO is also a major component of synthesis gas (syngas), where the relative amounts of CO and H₂ vary largely, depending on the feedstock, gasifier type and process conditions adopted (3). The release of CO into the atmosphere may have significantly negative environmental impact by affecting the abundance of greenhouse gases in the atmosphere.

The ability to grow on gaseous substrates as the sole carbon source is a defining property of the acetogens of the genus *Clostridium*, which use the carbon-fixation Wood-Ljungdahl biochemical pathway for autotrophic growth (4). Regeneration of redox cofactors occurs through reactions leading to excreted by-products. One such product of particular importance is 2,3-butanediol (2,3-BDO), a trace component of the native product profile of some C₁-fixing,

¹ Published as: Parsa, G., Angela, R., Luca, R., & Joshua, C. S. H. (2022). Metabolic Engineering Interventions for Sustainable 2,3-Butanediol Production in Gas-Fermenting *Clostridium autoethanogenum*. *MSystems*, 7(2), e01111-21. <https://doi.org/10.1128/msystems.01111-21>

anaerobic, acetogenic, ethanogenic, and carboxydrotrophic members of the genus *Clostridium*, namely *C. autoethanogenum*, *C. ljungdahlii*, *C. sp AWRP*, *C. ragsdalei* and *C. coskatii* (5-7).

2,3-BDO is a valuable platform chemical (8), which can be used to produce butadiene (a monomer of synthetic rubber), acetoin (a volatile compound used in foods, plant growth promoters, and biological pest control), diacetyl (a flavor enhancer), and methyl ethyl ketone (an excellent organic solvent). Furthermore, hydrogenation of methyl ethyl ketone produces the fuel 2-butanol, which shows the highest octane number and the lowest boiling point among the four stereoisomers of butanol. Compared to bioethanol, butanol has a higher energy density and lower hygroscopicity. Blending of 2-butanol with gasoline does not need to modify the current vehicle system (9). 2,3-BDO can be used as antifreeze agent because of the low freezing point shown by aqueous solutions of its stereoisomers (10-11), and as a novel chain initiator and extender in the manufacturing of polyol components of polyurethane foams (12). Furthermore, 2,3-BDO could be exploited in the cosmetics sector owing to its humectant, moisturizing and anti-microbial activities (13).

The initial reaction for the production of 2,3-BDO from acetyl-CoA is mediated by the pyruvate:ferredoxin oxidoreductase (PFOR), which is present in two copies in the genome of *C. autoethanogenum* (CAETHG_0928 and CAETHG_3029) (5,14-15). This enzyme catalyzes the interconversion of acetyl-CoA and CO₂ into pyruvate, with ferredoxin and thiamine pyrophosphate as cofactors (**Figure 1**). 2,3-BDO formation from pyruvate occurs through three subsequent reactions. Firstly, acetolactate synthase (ACLS), encoded by CAETHG_1740 in *C. autoethanogenum*, forms a molecule of acetolactate from two molecules of pyruvate, accompanied by the release of a CO₂ molecule. Acetolactate is then splitted into acetoin and CO₂ by acetolactate decarboxylase (ACLDC), encoded by CAETHG_2932 in *C. autoethanogenum*.

Acetoin can be finally reduced to 2,3-BDO by a butanol dehydrogenase (hereafter BTDDx), which is encoded by CAETHG_0385 in *C. autoethanogenum*, or by a primary-secondary alcohol dehydrogenase (hereafter BTDDy), which is encoded by CAETHG_0553 in *C. autoethanogenum* (16-17). It has been hypothesized that this primary-secondary NADPH-dependent alcohol dehydrogenase is also involved in ethanol production and not only in 2,3-BDO synthesis (18). Whereas this enzyme strictly depends on NADPH (17), the reduction of acetoin to 2,3-BDO by BTDDx is favored by NADH even if it has been observed both with NADPH and NADH (16).

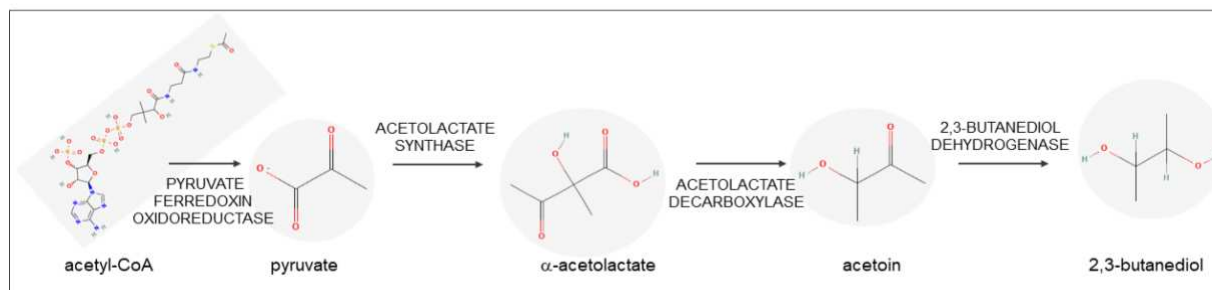


Figure 1. 2,3-butanediol biosynthetic pathway. Shown are the enzymes involved in the synthesis of 2,3-butanediol starting from acetyl-CoA.

Although 2,3-BDO production by microbial fermentation of gaseous substrates containing CO has been demonstrated (19), 2,3-BDO is usually a secondary product of gas fermentation processes. It is desirable to be able to affect the fermentation in such a way that the production of 2,3-BDO is enhanced relative to the production of other products, including ethanol, that are routinely produced in the fermentation of gaseous substrates by acetogens of the genus *Clostridium*. A few key process parameters have been identified as able to influence 2,3-BDO production. It has been shown that increasing the hydrogen composition of the gaseous substrate

and the specific rate of hydrogen consumption by the microbial culture negatively impacts on the 2,3-BDO productivity and that increasing the age of the cells in culture favors 2,3-BDO productivity (20). Medium manipulations included providing a compound inhibiting one or more enzymes, which convert acetolactate to branched chain amino acids to the fermentation (21) or increasing the concentration of at least one nutrient selected from the group consisting of vitamin B1, vitamin B5, vitamin B7 and mixtures thereof above the cellular requirement of the microorganism (22). A clear metabolic engineering strategy for increased 2,3-BDO production is not available despite the availability of genome-scale metabolic reconstructions of *C. autoethanogenum* (23-25) and the predictive engineering potential of constraint-based modeling (26), based on stoichiometry (27), and kinetic modeling, which allow to gain insights into regulatory behaviors or rate limiting steps (28). To avoid the hurdle of quantifying detailed enzyme kinetics of each reaction, which is impractical for large-scale networks, many frameworks explore a range of parameters and select a subset based on their consistency with experimental observations. Using the parameters obtained by training the model, the analysis of the network kinetics allows formulating potential engineering strategies. The ensemble modeling (EM) framework uses phenotypic data, such as flux changes due to changes in enzyme expression to screen for kinetic models. The EM approach builds up an ensemble of models that span the space of kinetics allowable by thermodynamic constraints and that would all reach the given steady state, when considering flux distribution and metabolite concentrations. The constructed models can then be employed to predict system phenotypes, such as flux changes due to changes in enzymes' expression levels (29). Cells are typically robust to perturbations to native enzyme concentrations. However, the addition of heterologous pathways may not result in similar steady-state stability. The robustness issue of non-natural pathways is addressed in

Ensemble Modeling for Robustness Analysis by computing the likelihood for an intervention to cause a metabolic instability (30). It is notable that available modeling tools increase the breadth of modeling techniques addressing the thermodynamic and kinetic feasibility of a metabolic pathway and its robustness against perturbations (31).

Metabolic engineering to obtain 2,3-BDO is currently limited by the fact that acetogens live at the thermodynamic edge of life (32). As shown in **Figure 2**, the Wood-Ljungdahl pathway, which acts as a terminal electron-accepting/energy-conserving process and as a mechanism for CO₂ assimilation into cell carbon (33), is neutral with respect to ATP production via substrate level phosphorylation (32), when acetyl-CoA is transformed into acetate (4). Consequently, autotrophic growth of acetogens of the genus *Clostridium* is strictly dependent on the chemiosmotic energy conservation process. The only coupling site for energy conservation is the Rnf complex whereby the free energy change of the electron transport is coupled to the extrusion of ions from the cytoplasm to the periplasm. The generated electrochemical ion gradient across the membrane drives ATP synthesis via a membrane-bound F₀F₁-ATP synthase (34).

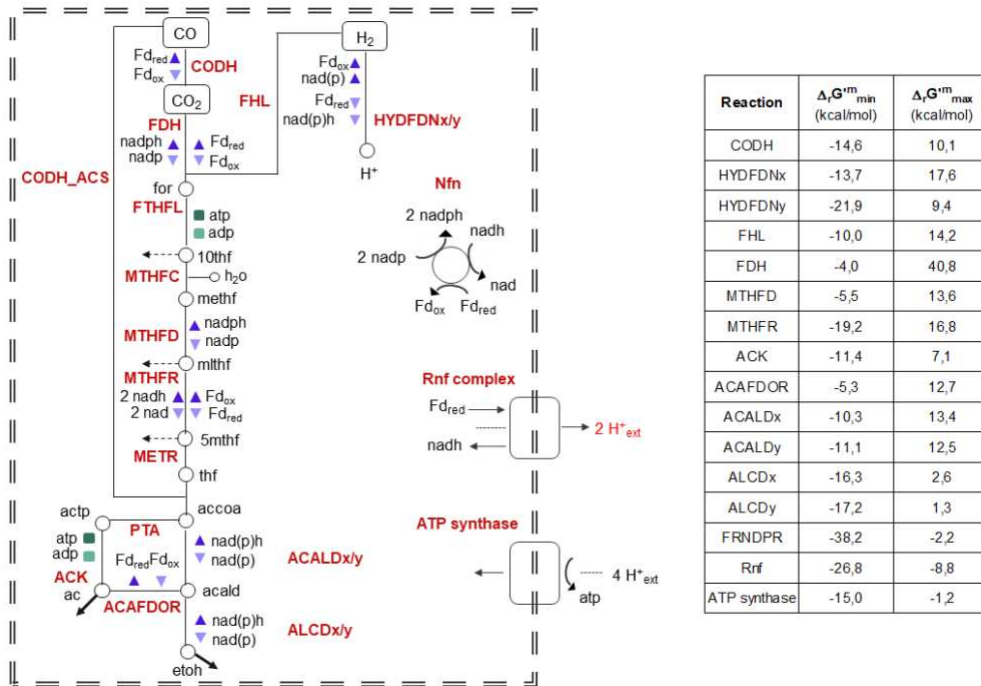


Figure 2. Bioenergetics in *C. autoethanogenum*. The reducing equivalents for the reductive steps during CO oxidation are provided by the carbon monoxide dehydrogenase, which reduces Fd. The electron-bifurcating and ferredoxin-dependent transhydrogenase Nfn is transferring electrons between Fd, NADH and NADPH. The methylene-THF reductase is assumed to be electron bifurcating. Excess Fd_{red} is oxidized by the Rnf complex, which reduces NAD and builds up a H⁺ gradient. This gradient drives ATP synthesis via the H⁺-dependent ATP synthase.

When using CO as the sole carbon source, in the absence of significant H₂, a fraction of CO is converted to CO₂ (35-37). The production of CO₂ represents inefficiency in the overall carbon capture and, if released, has the potential to contribute to greenhouse gas emissions.

This study aims at *in silico* identifying metabolic engineering interventions for increasing 2,3-BDO production and limiting the carbon loss in the form of CO₂ with a *C. autoethanogenum* culture fermenting a substrate comprising CO and H₂ by using constraint-based stoichiometric modeling and kinetic ensemble modeling.

Results and Discussion

Model validation. GEName-scale metabolic Models (GEMs) have been previously developed for *C. autoethanogenum*, namely iCLAU786 (32-33) and, more recently, Metaclau (34). Prior to the use of a GEM for *in silico* strain design, we developed a three-step benchmark (https://github.com/chan-csu/OptForce_Bdoh). In the first step, we looked for any internal flux after blocking all the exchange reactions. In the second step, we looked at flux through ATP hydrolysis reaction in the absence of any exchange fluxes. iCLAU786 failed both tests, while Metaclau succeeded in both cases. There was no flux-carrying reaction in the absence of exchange fluxes in Metaclau. However, there were many reactions with non-zero flux in iCLAU786 including the ATP hydrolysis reaction which shows infeasible energy-generating cycles. Presence of such cycles result in unrealistic simulation results. Finally, we assessed the accuracy of both genome-scale metabolic reconstructions by constraining each of them with experimental substrate uptake rates, and by evaluating the ability of the models to predict experimentally observed biomass and by-products' production rates. We retrieved the experimental datasets for validation purposes from research articles, which explore gas fermentations using *C. autoethanogenum* grown on CO-rich gas substrates and which report quantitative data on gas uptake and production rates (**Table 1**). We constrained the metabolic reconstructions with the gas uptake rates corresponding to each gas fermentation condition, shown in **Table 1**, and we carried out Flux Balance Analysis (FBA) as well as Flux Variability Analysis (FVA) simulations by maximizing biomass yield. The accuracy in predicting the acetate, ethanol and 2,3-BDO production rates and the specific growth rate was found to be superior using Metaclau compared to iCLAU786. A possible reason for the better performance of Metaclau is its better model consistency since it does not contain the aforementioned energy-

generating cycles. Based on the assessment of Metaclau prediction accuracy by FBA and FVA simulations (**Figure 3**), we used the Metaclau GEM in the following *in silico* analysis.

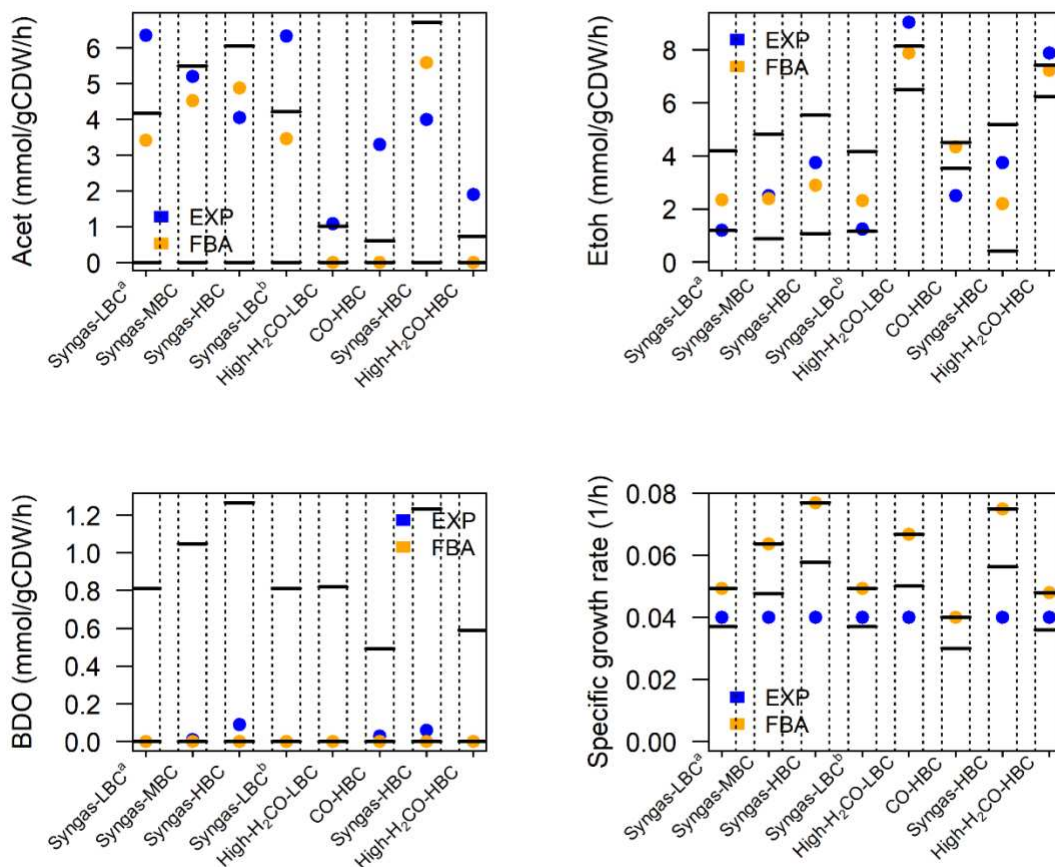


Figure 3. Validation of Metaclau predictive capability by contrasting FBA and FVA predictions with experimentally determined production rates in benchmarking datasets.

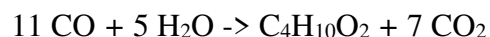
The plots show the experimental acetate, ethanol, 2,3-BDO production rates and specific growth rate (blue dots), which are reported in **Table 1**, with the flux predictions obtained by FBA (orange dots) and with the flux ranges which were obtained by FVA simulations using the Metaclau GEM, constrained with the experimental gas uptake rates in **Table 1**.

Table 1. Quantitative datasets for model validation. Shown are the gas substrate uptake rates and production rates, which were displayed in publicly available reports on quantitative gas fermentations based on CO-rich gas substrates and reliant on *C. autoethanogenum*. The table shows the composition of the gas substrate for each experiment. LBC, MBC and HBC stand for low, medium and high biomass concentration

Reference	Gas substrate	Biomass concentration	Gas substrate composition	q _{CO} (mmol/g _C DW/h)	q _{CO₂} (mmol/g _C DW/h)	q _{H₂} (mmol/g _C DW/h)	q _{Acet} (mmol/g _C DW/h)	q _{etoh} (mmol/g _C DW/h)	q _{BDO} (mmol/g _{CDW} /h)	μ (h ⁻¹)				
Valgepea 2017	Syngas ^a	LBC	50% CO;20% CO ₂ ;20% H ₂ ;10% Ar	-	18.8	5.65	-12.6	6.35	1.2	0	0.04			
Valgepea 2017	Syngas	MBC	50% CO;20% CO ₂ ;20% H ₂ ;10% Ar	-	24.6	8.7	-12.5	5.2	2.5	0.01	0.04			
Valgepea 2017	Syngas	HBC	50% CO;20% CO ₂ ;20% H ₂ ;10% Ar	-	30.6	12.5	5	-11.9	4.05	3.7	5	0.09	0.04	
Valgepea 2018	Syngas ^b	LBC	50% CO;20% CO ₂ ;20% H ₂ ;10% Ar	-	18.7	5.62	5	-	6.33	3	5	0	0.04	
Valgepea 2018	High -H ₂ CO	LBC	15% CO;45% H ₂ ;40% Ar	-	20.0	2.12	5	-	1.08	9.0	3	42	0	0.04
Valgepea 2018	CO	HBC	60% CO;40% Ar	-	-31	21	0.5	3.3	2.5	0.03			0.04	
Valgepea 2018	Syngas	HBC	50% CO;20% CO ₂ ;20% H ₂ ;10% Ar	-	-30	12	-11	4	3.7	5	0.06		0.04	

Valgep	High		15%								
ea	-H ₂		CO;45%						7.8		0.04
2019	CO	HBC	H ₂ ;40% Ar	-20	4	-29	1.9	8	0		

Analysis of the effect of H₂ on 2,3-butanediol and CO₂ production. CO represents a carbon source that provides reducing equivalents via CO oxidation through a water gas shift reaction catalyzed by carbon monoxide dehydrogenase (CODH). However, the usage of CO as electron donor is associated with the release of CO₂ (35-37). For example, when using only CO for 2,3-BDO production, almost two-thirds of the carbon is lost to CO₂ according to:



Since we were interested in identifying metabolic engineering strategies to improve 2,3-BDO production in a gas feeding condition minimizing CO₂ production, we explored feed gas substrates combining CO with H₂. Indeed, if H₂ is present in the gas, additional reducing equivalents are made available by hydrogen oxidation ($\text{H}_2 \rightarrow 2 \text{ H}^+ + 2e^-$) and less CO has to be dissipated into CO₂ via the biological water gas shift catalyzed by CODH. Furthermore, CO₂ can be advantageously fixed in the Wood-Ljungdahl pathway since the direct use of H₂ in the CO₂ reduction to formate by the formate-hydrogen lyase activity (16) allows to save redox compared to growth on CO alone. A high-H₂/CO gas fermentation process using chemostat cultures of *C. autoethanogenum* (38) observed the aforementioned trend whereby the specific CO₂ production rate dropped more than fivefold by increasing the supplied H₂. Our FVA simulations predicted a significant drop of CO₂ production rate from 21 mmol/g_{CDW}/h, when CO was the sole gas substrate in the Metaclau GEM, to 2 mmol/g_{CDW}/h, when the Metaclau GEM was constrained with the CO and H₂ uptake rates corresponding to the high-H₂/CO gas feeding adopted in ref. 38. Running FVA simulations for different combinations of CO and H₂ uptake rates allowed us to

identify a subspace of gas uptake rates' combinations that ensure 2,3-BDO production and that substantially decrease CO₂ production (**Supplementary Figure 1**). We ran another simulation using the kinetic ensemble model of the *C. autoethanogenum* core metabolism derived in ref. 42, where we held the CO uptake constant and we varied the H₂ uptake rate. We did observe a decrease in the 2,3-BDO yield per hydrogen uptake. Especially after the uptake rate of hydrogen is > 20 mmol/gDW/hr, no increase in 2,3-BDO or any other significant product profile change was observed (**Supplementary Figure 2**). The additional electrons at high hydrogen uptake are consumed in some futile cycles in the model. The primary reason for this model behavior is that all kinetics in the model essentially follow Michaelis-Menten kinetics and the hydrogen-consuming reactions that lead to product formation will ultimately get saturated at a certain hydrogen concentration that is correlated to the H₂ uptake rate. In the light of this behavior at higher simulated H₂ uptakes, we constrained the GEM with the particular combination of CO and H₂ uptake rates reported in ref. 38 which have been experimentally shown to be associated with a low CO₂ production rate, in order to computationally predict metabolic interventions enhancing 2,3-BDO production rate at low CO₂ production rate.

Prediction of genetic manipulations leading to 2,3-butanediol overproduction. The OptForce framework (39) implemented within the COBRA toolbox (40) in MATLAB environment was used with the Metaclau GEM to enumerate the reactions that should be actively forced through genetic interventions in order to achieve the overproduction of 2,3-BDO in *C. autoethanogenum* fed with CO and H₂. Optforce allowed us to retrieve single, double and triple interventions reported in **Supplementary File 2** (https://github.com/chan-csu/OptForce_Bdoh/raw/master/Results/Supplementary_Table_1.xlsx). Each intervention can foresee the increase, decrease or elimination of the flux value corresponding to each of the

Ensemble Modeling approach does not require the existence neither of metabolomics data nor of enzymatic expression data but builds upon a reference steady-state flux distribution to constrain the kinetic parameters' sampling space to a realistic space and, thus, to derive the initial ensemble of multiple kinetic parameter sets. This ensemble is subsequently pruned down using perturbation datasets, which typically consist of phenotypic responses to enzymatic modifications. In ref. 42, the screening of the ensemble of kinetic parametric sets did not rely on genetic perturbations, for which available data are currently limited in *C. autoethanogenum*, but on perturbations of environmental conditions. Indeed, the construction of the kinetic model relied on a public dataset where gas uptake fluxes changed by effect of increasing the biomass concentration over three conditions (45). Eighteen sets of locally stable kinetic parameters fit the experimental data in all three conditions. We used this ensemble model consisting of the 18 sets of parameters for our simulations.

The kinetic ensemble model of *C. autoethanogenum* was instrumental to elucidate the change in 2,3-BDO production rate as a function of changing the expression levels of the enzymes catalyzing the reactions, which took part in the interventions suggested by Optforce. In particular, we simulated multiple scenarios where the fold changes of the enzymes catalyzing each reaction of the single, double or triple interventions were set to low ($\pm 20\%$), medium ($\pm 40\%$) or high ($\pm 60\%$). Each intervention is associated with a distribution of 2,3-BDO production rates which resulted from simulating all the 18 sets of kinetic parameters of the ensemble model (42). The distribution of the simulated 2,3-BDO production rates relative to each single, double and triple intervention are shown respectively in **Figures 5, 6, and 7**. We then identified the interventions that resulted in significantly higher production of 2,3-BDO

compared to the wild-type condition (Wilcoxon’s test, significance level at 1%). **Tables 2, 3, 4** reported the reactions involved in statistically significant single, double or triple interventions, respectively. We also tested the effects of larger perturbations. We repeated the simulations to perturb the enzyme levels by 3, 5 and 10 folds for upregulation and 0.3, 0.2, and 0.1 fold change for downregulation. The same strategies were suggested to increase 2,3-BDO production most significantly.

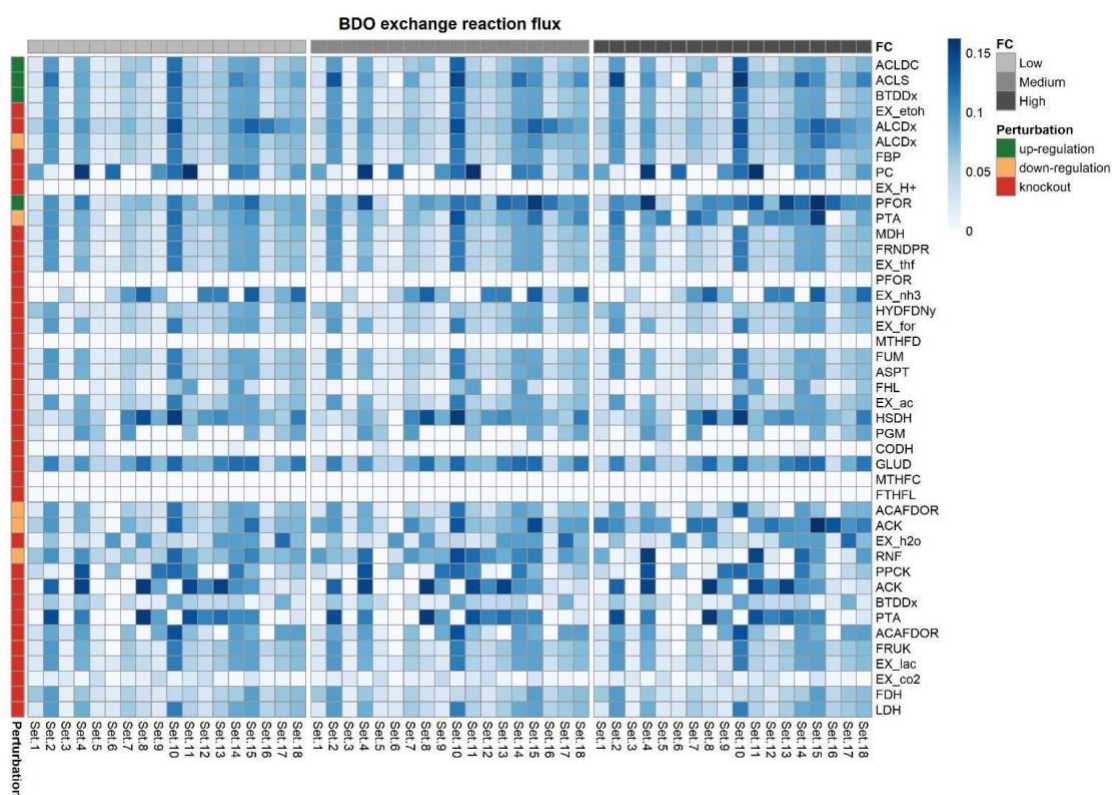


Figure 5. Heatmap showing the 2,3-BDO production rate when each of the single interventions suggested by Optforce are applied to the kinetic core model. Each row in the heatmap represents an intervention and each column represents one of the 18 kinetic parameters sets. The intervention can be an up-regulation, a down-regulation or a knockout. The heatmap is column wise subdivided in three blocks. Each block corresponds to different extents in the change of the levels of the enzymes catalyzing each reaction. We referred to the fold changes in enzymes’ expression levels as to low, medium, and high, respectively.

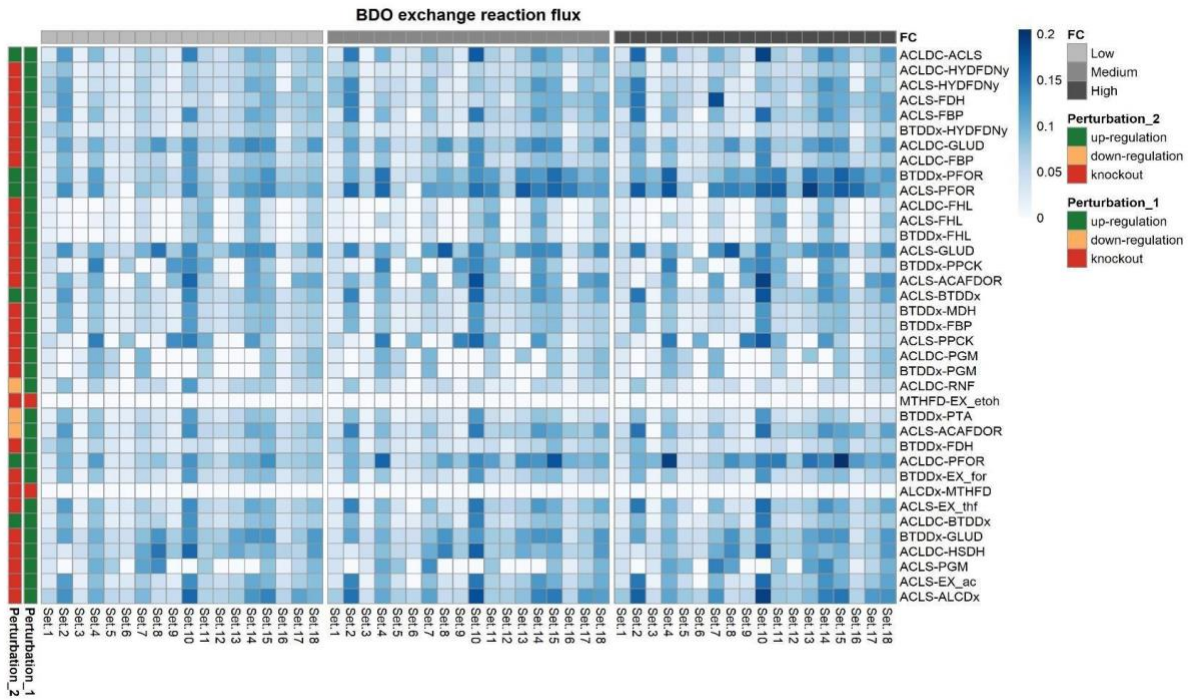


Figure 6. Heatmap showing the 2,3-BDO production rate when each of the double interventions suggested by Optforce is applied to the kinetic core model. Each row in the heatmap represents a double intervention and each column represents one of the 18 kinetic parameters sets. The perturbation applied to each reaction included in a double intervention be an up-regulation, a down-regulation or a knockout. The heatmap is column wise subdivided in three blocks. Each block corresponds to different extents in the change of the levels of the enzymes catalyzing each reaction of the double intervention. We referred to the fold changes in enzymes' expression levels as to low, medium and high, respectively.

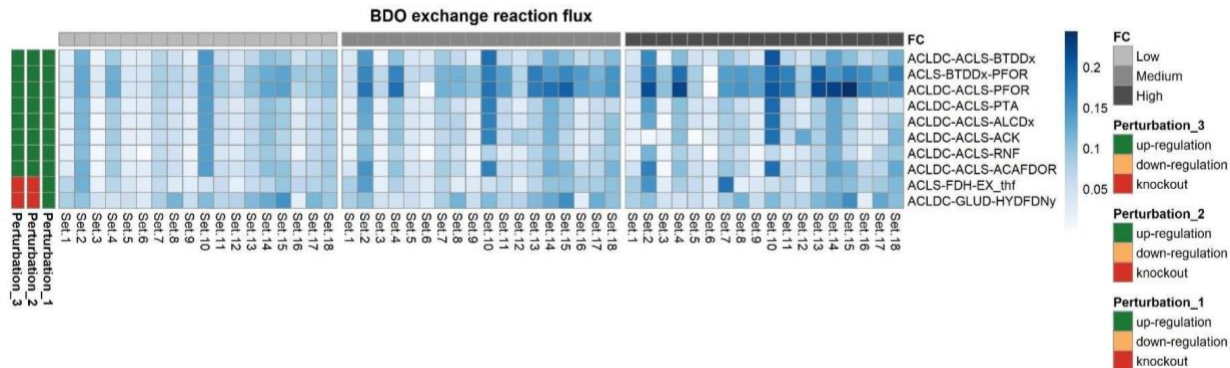


Figure 7. Heatmap showing the 2,3-BDO production rate when each of the triple interventions suggested by Optforce are applied to the kinetic core model. Each row in the heatmap represents a triple intervention and each column represents one of the 18 kinetic parameters sets. The perturbation applied to each reaction included in a triple intervention can be an up-regulation, a down-regulation or a knockout. The heatmap is column wise subdivided in three blocks. Each block corresponds to different extents in the change of the levels of the enzymes catalyzing each reaction of the triple intervention. We referred to the fold changes in enzymes' expression levels as to low, medium and high, respectively.

PFOR up-regulation predicted to be the most effective single intervention. First-order interventions which were predicted to increase 2,3-BDO production, compared to the wild-type (WT) condition, primarily concern the up-regulation of enzymes involved in the 2,3-BDO biosynthetic pathway. As shown in **Figure 8**, overexpressing pyruvate:ferredoxin oxidoreductase (PFOR), which catalyses the interconversion between acetyl-CoA and pyruvate, was predicted to be the most effective single intervention for improving 2,3-BDO synthesis ($flux_{PFOR\ up,high}^{2,3-BDO} = 0.10 \pm 0.023$; $flux_{WT}^{2,3-BDO} = 0.039 \pm 0.0091$), followed by the up-regulation of acetolactate synthase (ACLS) ($flux_{ACLS\ up,low}^{2,3-BDO} = 0.073 \pm 0.032$). PFOR up-regulation was predicted to lead to a 2.6-fold increase in 2,3-BDO production rate. This reaction has previously been identified to be the rate limiting step in 2,3-BDO formation in *C. autoethanogenum* (46). Therein, the authors assayed the activity of the oxidoreductase enzymes involved in the Wood-Ljungdahl

pathway and in the fermentation pathway to 2,3-BDO using *C. autoethanogenum*, grown autotrophically with a feeding gas composed of 2% H₂, 42% CO, 20% CO₂ and 36% N₂. Measurements showed at least an activity of 1.1 U/mg for the assayed reactions, whereas the PFOR rate limiting reaction exhibited an enzyme activity of only 0.11 U/mg in the presence of ferredoxin, corresponding to 90% less than all other reactions assayed. PFOR overexpression was found to increase the flux through pyruvate and to increase 2,3-BDO production (46). This indicates that the ensemble kinetic model did capture some kinetic information beyond the stoichiometric model that is consistent with experimental results.

As shown in **Figure 8**, an alternative kind of intervention to increase the 2,3-BDO production acts on the pathway leading to acetate and, ultimately, ethanol formation. Indeed, the knockout or down-regulation of ethanol:NAD oxidoreductase (ALCDx), the phosphate acetyltransferase (PTA) down-regulation and the acetate kinase (ACK) down-regulation were predicted to increase 2,3-BDO production ($flux_{ALCDx\ KO}^{2,3-BDO} = 0.070 \pm 0.025$; $flux_{ALCDx\ down,high}^{2,3-BDO} = 0.066 \pm 0.024$; $flux_{PTA\ down,medium}^{2,3-BDO} = 0.087 \pm 0.030$; $flux_{ACK\ down,high}^{2,3-BDO} = 0.098 \pm 0.017$). PTA and ACK down-regulations were predicted to result, respectively, in a 2.23-fold and 2.51-fold increase in 2,3-BDO production rate. Upon PTA and ACK down-regulation, the flux through acetaldehyde:ferredoxin oxidoreductase (ACAFDOR) decreases respectively by 3.89-fold and by more than 5-fold compared to the wild type case, thus limiting the consumption of reduced ferredoxin, which in turn causes the NADP to be regenerated (reduced) to NAD(P)H. The latter builds an excess that must be relieved to equilibrium, and, in doing so, reduces acetoin to 2,3-BDO. Furthermore, the slight increase in 2,3-BDO production rate could be due to the flux decrease which is generally observed through the gluconeogenesis pathway, upon both PTA and ACK down-regulation. PTA down-regulation negatively affects also the incomplete TCA cycle.

Interestingly, PTA and ACK down-regulations were among the rare cases where the level of change in enzyme expression was predicted by the kinetic ensemble model to influence the effect size on 2,3-BDO production, with only a moderate phosphate acetyltransferase and acetate kinase down-regulation found effective. This outcome could be explainable by the key role of the conversion of acetyl-CoA to acetate via acetyl-phosphate for ATP production in the energy metabolism of acetogens (47). This also highlights the importance of an accurate quantitative model for effective optimization of gene expression. Unless differently specified, hereafter we report the 2,3-BDO production rates, which were estimated by simulating the highest change in the expression levels of the enzymes involved in each intervention.

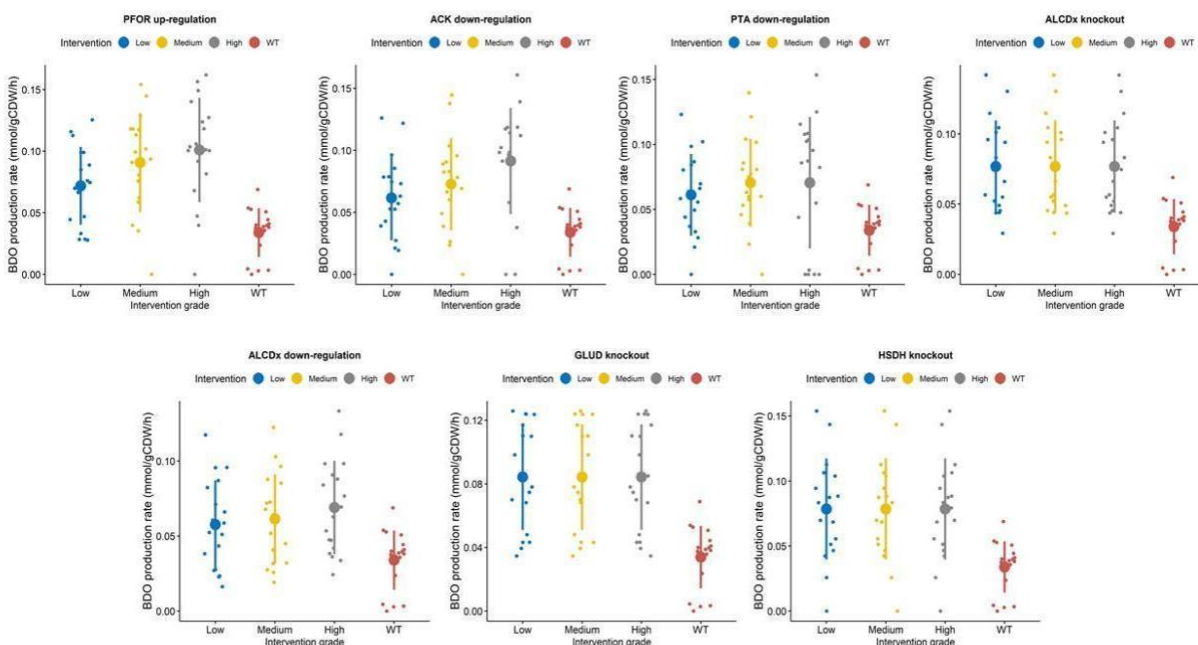


Figure 8. Plots showing the distribution of 2,3-BDO production rates across 18 kinetic parametric sets, under the wild-type scenario and under the single modification scenario. For each intervention, three (low, medium and high) fold changes were simulated. Overlaid are the mean and standard deviation of the 2,3-BDO production rates corresponding to each intervention at each simulated change in gene expression. The figure only refers to selected single interventions reported in **Table 2**.

Table 2. Summary of first order interventions validated by the kinetic model of *C. autoethanogenum*. Shown are the single interventions which result in a statistically significant higher 2,3-BDO production rate compared to the wild-type condition (Wilcoxon' test, significance level at 1%).

Reaction	Intervention	Adjusted P-value		
		Low	Medium	High
ALCDx <i>nadh + h + acald <=> nad + etoh</i>	knock-out	1,64E-04	1,64E-04	1,64E-04
PFOR <i>coa + pyr + Fd_ox <=> co2 + accoa + h + Fd_red</i>	up-regulation	1,64E-03	1,64E-03	1,64E-04
GLUD <i>h2o + nadp + glu-L <=> nadph + nh3 + akg + h</i>	knock-out	1,64E-04	1,64E-04	1,64E-04
ALCDx <i>nadh + h + acald <=> nad + etoh</i>	down-regulation	5,41E-03	2,30E-03	4,92E-04
ACK <i>adp + actp <=> atp + ac + h</i>	down-regulation	8,20E-04	4,92E-04	4,92E-04
ACLS <i>2 pyr + h <=> co2 + acltt</i>	up-regulation	4,10E-03	2,30E-03	8,20E-04

HSDH	knock-out	4,10E-03	4,10E-03	4,10E-03
$nad + hom-L \rightleftharpoons nadh + h + aspsa$				
HYDFDNy	knock-out	7,05E-03	7,05E-03	7,05E-03
$nadp + Fd_{ox} + 2 h2 \rightleftharpoons nadph + 3 h + Fd_{red}$				
PTA	down-regulation	1,64E-03	1,64E-04	7,23E-02
$pi + accoa + h \rightleftharpoons coa + actp$				
RNF	down-regulation	1,64E-04	2,30E-03	1,00E+00
$nad + 3 h + Fd_{red} \rightleftharpoons nadh + 2 h_{ext} + Fd_{ox}$				

The benefit induced by the knockout of ALCDx, which catalyses the NAD-dependent conversion of acetaldehyde into ethanol, is probably attributable to the negation of a competitive reaction for the electrons required for 2,3-BDO in the form of NADH. Indeed, the flux through the NAD-dependent butanediol dehydrogenase increases of 29 %. Furthermore, the ALCDx knockout induces a 2.78-fold higher flux through the NADP-dependent acetaldehyde dehydrogenase (ACALDy), which operating in the opposite direction relative to ethanol formation, increases the acetyl-CoA pool for PFOR whose flux increases of 14%.

Overexpression of both PFOR and ACLS predicted as the most effective double intervention. Enhancing the expression of multiple enzymes involved in the 2,3-BDO biosynthetic pathway appears as a relevant choice in double interventions (**Figure 9**). Many of

the double interventions rely on the enzymes highlighted in the analysis of single interventions and propose the combined intervention on two of such enzymes. Notably, our analysis revealed that the preferable enzyme to overexpress along with PFOR is ACLS, which lies immediately downstream to pyruvate oxidoreductase and converts pyruvate to acetolactate and carbon dioxide. This double intervention resulted in 1.4-fold higher 2,3-BDO production rate compared to overexpressing only the pyruvate oxidoreductase gene, with a 3.59-fold higher 2,3-BDO production rate compared to the wild-type condition ($flux_{ACLS\ up, PFOR\ up}^{2,3-BDO} = 0.14 \pm 0.030$). On the contrary, overexpressing both PFOR and BTDDx or PFOR and ACLDC resulted in an almost identical 2,3-BDO production rate than just overexpressing the PFOR gene alone ($flux_{BTDDx\ up, PFOR\ up}^{2,3-BDO} = 0.11 \pm 0.026$; $flux_{PFOR\ up, ACLDC\ up}^{2,3-BDO} = 0.11 \pm 0.030$). These findings highlight the benefit of combining Optforce with the kinetic ensemble model since kinetic models parameterized from experimental data can help identify the possible kinetic bottlenecks inside a metabolic pathway among the interventions suggested by OptForce that are equivalent at the stoichiometric level.

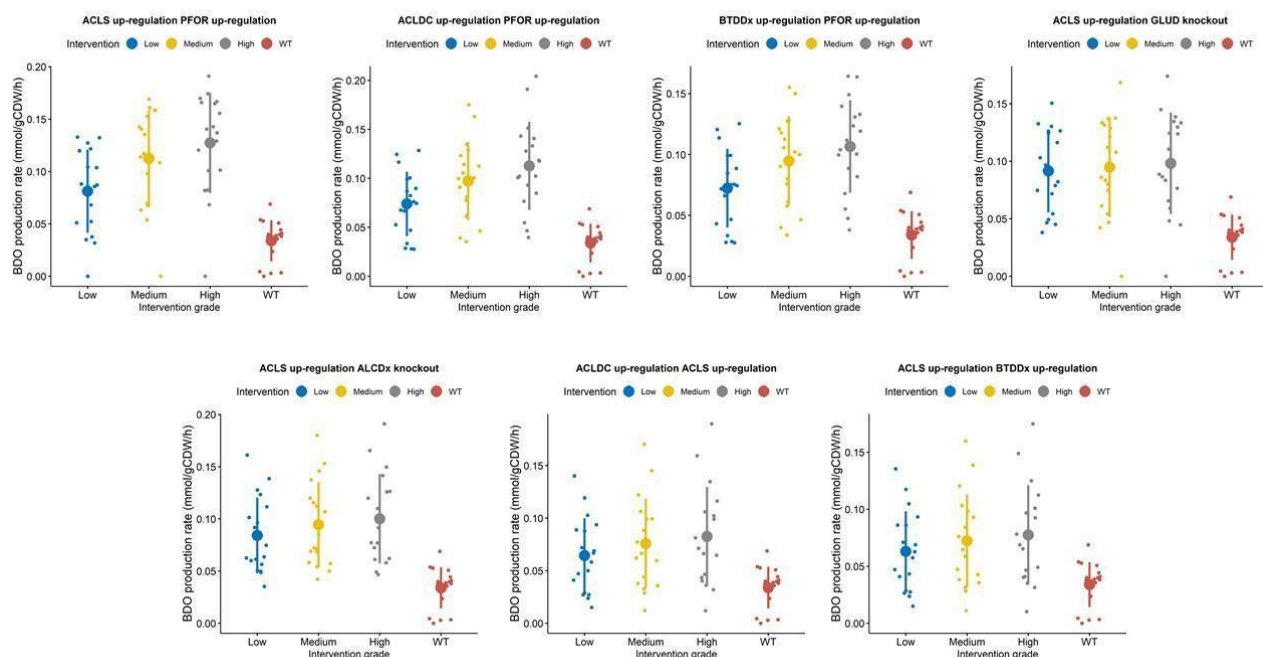


Figure 9. Plots showing the distribution of 2,3-BDO production rates across 18 kinetic parametric sets, under the wild-type scenario and under the double modification scenario. For each gene involved in a double intervention, three (low, medium and high) fold changes were simulated. Overlaid are the mean and standard deviation of the 2,3-BDO production rates corresponding to each intervention at each simulated change in gene expression. The figure only refers to selected double interventions reported in **Table 3**.

Table 3 Summary of second order interventions validated by the kinetic model of *C. autoethanogenum*. Shown are the double interventions which result in a statistically significant higher 2,3-BDO production rate compared to the WT (Wilcoxon' test, significance level at 1%).

1st reaction	1st intervention	2nd reaction	2nd intervention	Adjusted P-value		
				Low	Medium	High
ACLS	up-regulation	PFOR	up-regulation	1,41E-03	1,41E-04	1,41E-04

$2 \text{ pyr} + h$ $\langle \Rightarrow \rangle \text{ co2}$ $+ \text{ acltt}$	$\text{coa} + \text{pyr} + \text{Fd}_{ox}$ $\langle \Rightarrow \rangle \text{ co2} + \text{accoa} +$ $h + \text{Fd}_{red}$					
ACLDC	up-regulation	PFOR	up-regulation	7,06E-04	2,68E-03	1,41E-04
$h + \text{acltt}$ $\langle \Rightarrow \rangle \text{ co2}$ $+ \text{actn}$	$\text{coa} + \text{pyr} + \text{Fd}_{ox}$ $\langle \Rightarrow \rangle \text{ co2} + \text{accoa} +$ $h + \text{Fd}_{red}$					
ACLS	up-regulation	ALCDx	knock-out	1,41E-04	1,41E-04	1,41E-04
$2 \text{ pyr} + h$ $\langle \Rightarrow \rangle \text{ co2}$ $+ \text{acltt}$	$\text{nadh} + h + \text{acald}$ $\langle \Rightarrow \rangle \text{ nad} + \text{etoh}$					
ACLDC	up-regulation	ACLS	up-regulation	1,98E-03	1,41E-03	2,82E-04
$h + \text{acltt}$ $\langle \Rightarrow \rangle \text{ co2}$ $+ \text{actn}$	$2 \text{ pyr} + h \langle \Rightarrow \rangle \text{ co2} +$ acltt					
ACLS	up-regulation	HYDFDNy	knock-out	7,06E-04	2,82E-04	2,82E-04
$2 \text{ pyr} + h$ $\langle \Rightarrow \rangle \text{ co2}$ $+ \text{acltt}$	$\text{nadp} + \text{Fd}_{ox} + 2 \text{ h2}$ $\langle \Rightarrow \rangle \text{ nadph} + 3 \text{ h} +$ Fd_{red}					
ACLDC	up-regulation	GLUD	knock-out	2,82E-04	2,82E-04	2,82E-04
$h + \text{acltt}$ $\langle \Rightarrow \rangle \text{ co2}$ $+ \text{actn}$	$\text{h2o} + \text{nadp} + \text{glu-L}$ $\langle \Rightarrow \rangle \text{ nadph} + \text{nh3} +$ $\text{akg} + h$					
BTDDx	up-regulation	PFOR	up-regulation	1,41E-03	1,98E-03	2,82E-04

<i>nad</i> + <i>bdoh</i> <=> <i>nadh</i> + <i>h</i> + <i>actn</i>		<i>coa</i> + <i>pyr</i> + <i>Fd_ox</i> <=> <i>co2</i> + <i>accoa</i> + <i>h</i> + <i>Fd_red</i>				
ACLS	up- regulati on	GLUD	knock-out	1,41E-04	7,06E-04	2,82E-04
<i>2 pyr</i> + <i>h</i> <=> <i>co2</i> + <i>acltt</i>		<i>h2o</i> + <i>nadp</i> + <i>glu-L</i> <=> <i>nadph</i> + <i>nh3</i> + <i>akg</i> + <i>h</i>				
ACLS	up- regulati on	BTDDx	up- regulation	4,66E-03	1,98E-03	2,82E-04
<i>2 pyr</i> + <i>h</i> <=> <i>co2</i> + <i>acltt</i>		<i>nad</i> + <i>bdoh</i> <=> <i>nadh</i> + <i>h</i> + <i>actn</i>				
ACLS	up- regulati on	ACAFDOR	down- regulation	2,68E-03	7,06E-04	2,82E-04
<i>2 pyr</i> + <i>h</i> <=> <i>co2</i> + <i>acltt</i>		<i>ac</i> + 3 <i>h</i> + <i>Fd_red</i> <=> <i>h2o</i> + <i>acald</i> + <i>Fd_ox</i>				
BTDDx	up- regulati on	GLUD	knock-out	2,82E-04	1,41E-03	2,82E-04
<i>nad</i> + <i>bdoh</i> <=> <i>nadh</i> + <i>h</i> + <i>actn</i>		<i>h2o</i> + <i>nadp</i> + <i>glu-L</i> <=> <i>nadph</i> + <i>nh3</i> + <i>akg</i> + <i>h</i>				
ACLS	up- regulati on	FDH	knock-out	2,68E-03	2,68E-03	7,06E-04
<i>2 pyr</i> + <i>h</i> <=> <i>co2</i> + <i>acltt</i>		<i>nadph</i> + 2 <i>co2</i> + <i>h</i> + <i>Fd_red</i> <=> <i>nadp</i> + 2 <i>for</i> + <i>Fd_ox</i>				

ACLS	up-regulation	FBP	knock-out	3,53E-03	3,53E-03	7,06E-04
$2 \text{ pyr} + h$ $\langle \Rightarrow \rangle \text{ co2}$ $+ \text{ acltt}$		$h2o + fdp \langle \Rightarrow \rangle pi + h + f6p$				
ACLS	up-regulation	EX_thf	knock-out	3,53E-03	3,53E-03	7,06E-04
$2 \text{ pyr} + h$ $\langle \Rightarrow \rangle \text{ co2}$ $+ \text{ acltt}$		$thf - \rangle$				
ACLS	up-regulation	EX_ac	knock-out	3,53E-03	3,53E-03	7,06E-04
$2 \text{ pyr} + h$ $\langle \Rightarrow \rangle \text{ co2}$ $+ \text{ acltt}$		$ac_ext - \rangle$				
ACLDC	up-regulation	HSDH	knock-out	1,98E-03	4,66E-03	2,68E-03
$h + \text{ alctt}$ $\langle \Rightarrow \rangle \text{ co2}$ $+ \text{ actn}$		$nad + hom-L \langle \Rightarrow \rangle nadh + h + \text{ aspsa}$				
ACLDC	up-regulation	HYDFDNy	knock-out	4,66E-03	4,66E-03	3,53E-03
$h + \text{ alctt}$ $\langle \Rightarrow \rangle \text{ co2}$ $+ \text{ actn}$		$nadp + Fd_ox + 2 h2 \langle \Rightarrow \rangle nadph + 3 h + Fd_red$				
BTDDx	up-regulation	HYDFDNy	knock-out	9,88E-03	9,88E-03	9,88E-03
$nad + \text{ bdoh}$ $\langle \Rightarrow \rangle$		$nadp + Fd_ox + 2 h2 \langle \Rightarrow \rangle nadph + 3 h + Fd_red$				

nadh + h
+ actn

Among the double interventions which do not encompass PFOR, our analysis suggested firstly the combined overexpression of ACLS and BTDDx, and secondly the overexpression of ACLS and ACLDC, which ensure an around twofold higher 2,3-BDO production rate compared to the wild-type condition ($flux_{BTDDx\ up, ACLS\ up}^{2,3-BDO} = 0.073 \pm 0.030$; $flux_{ACLDC\ up, ACLS\ up}^{2,3-BDO} = 0.076 \pm 0.031$). ACLS and ACLDC were overexpressed individually and in combination in a patent of the Lanzatech company (46), whereby the combined intervention allowed to experimentally observe increased 2,3-BDO production in a batch culture of *C. autoethanogenum* using a CO-containing gas substrate. However, according to the outcomes of our *in silico* analysis, the double intervention did not lead to a tangible increase in 2,3-BDO production rate compared to overexpressing exclusively the acetolactate synthase whereas, according to ref. 46, the increase in 2,3-BDO production is primarily associated with the overexpression of the acetolactate decarboxylase.

Our analysis predicted that a 2.56-fold increase in 2,3-BDO production rate compared to the wild-type case could be achievable through a double intervention whereby the acetolactate synthase overexpression is combined with the knockout of glutamate dehydrogenase (GLUD), which catalyses the NADPH-dependent interconversion between L-glutamate and 2-oxoglutarate ($flux_{ACLS\ up, GLUD\ KO}^{2,3-BDO} = 0.10 \pm 0.034$). It has been shown that *C. autoethanogenum* contains a strictly NADPH-dependent primary-secondary alcohol dehydrogenase which could reduce acetoin to 2,3-BDO (17). Therefore, the suggested knockout of GLUD in conjunction with

ACLS up-regulation could favour 2,3-BDO production by avoiding NADPH consumption in the reaction catalyzed by glutamate dehydrogenase.

A slightly less effective intervention foresaw the ACLS upregulation combined with the ethanol:NAD oxidoreductase (ALCDx) knockout ($flux_{ACLS\ up, ALCDx\ KO}^{2,3-BDO} = 0.084 \pm 0.031$). The beneficial effect on 2,3-BDO production rate is probably attributable to the negation of a competitive reaction for the electrons required for 2,3-BDO in the form of NADH.

Another double intervention featured the combination of ACLS up-regulation with formate dehydrogenase (FDH) knockout ($flux_{ACLS\ up, FDH\ KO}^{2,3-BDO} = 0.074 \pm 0.032$). Its mode of action is likely based on the manipulation of the NAD(P)H to NAD(P) ratio. Indeed, knocking out FDH affords reduced ferredoxin to build up. This excess reduced ferredoxin causes the NADP to be regenerated (reduced) to NAD(P)H, which builds an excess that must be relieved to equilibrium, and reduces acetoin to 2,3-BDO. This is supported by the fact that the flux through the NADH-dependent BTDDx increases by 26% compared to the wild-type condition.

Also the double intervention consisting of ACLS up-regulation and ACAFDOR down-regulation is related to the provision of reduced ferredoxin since ACAFDOR down-regulation allows to limit the consumption of reduced ferredoxin ($flux_{ACLS\ up, ACAFDOR\ down}^{2,3-BDO} = 0.073 \pm 0.028$).

An alternative intervention foresaw the simultaneous up-regulation of ACLS and the knockout of the rate-limiting step in gluconeogenesis catalysed by fructose-bisphosphatase (FBP), which converts D-fructose-1,6-bisphosphate (fdp) into D-fructose-6-phosphate (f6p) and which was found to afford an almost 2-fold increase compared to the WT case ($flux_{ACLS\ up, FBP\ KO}^{2,3-BDO} = 0.074 \pm 0.032$). Based on the changes in flux distribution observed upon this intervention, FBP knockout restricts biomass formation since fdp is rerouted from f6p to D-fructose-1-phosphate

(f1p) through the action of fructose-1-phosphate kinase (FRUK). The advantage conferred to 2,3-BDO production by this intervention could derive firstly from the generation of ATP associated with the conversion of fdp into f1p, and, secondly, from an increased pyruvate pool made available for 2,3-BDO through D-fructose transport via the phosphoenolpyruvate:pyruvate phosphotransferases, FRUpts and FRUpts2.

Overexpression of ACLDC on top of PFOR and ACLS predicted to be the most effective triple intervention. When we explored the effectiveness of triple interventions, we interestingly

noted that the up-regulation of the entire branch from pyruvate to 2,3-BDO alone, i.e., acetolactate decarboxylase (ACLDC), acetolactate synthase (ACLS), and butanediol dehydrogenase (BTDDx), worsens the 2,3-BDO production rate compared to overexpressing pyruvate:ferredoxin oxidoreductase alone ($flux_{ACLDC\ up, ACLS\ up, BTDDx\ up}^{2,3-BDO} = 0.075 \pm 0.031$).

Overexpressing BTDDx on top of the simultaneous ACLS and PFOR up-regulation did not improve 2,3-BDO production compared to the double intervention (

$flux_{ACLS\ up, BTDDx\ up, PFOR\ up}^{2,3-BDO} = 0.14 \pm 0.029$). On the other hand, the up-regulation of

ACLDC on top of that of PFOR and ACLS resulted in the most effective triple intervention,

further boosting the 2,3-BDO production rate by about 7% with respect to the combined PFOR and ACLS up-regulation, and leading to an almost 4-fold increase in 2,3-BDO production

compared to the wild-type condition ($flux_{ACLDC\ up, ACLS\ up, PFOR\ up}^{2,3-BDO} = 0.15 \pm 0.056$). A strain

overexpressing all the three genes was characterized in continuous cultures grown on a CO-

containing gaseous substrate and consistently produced higher 2,3-BDO levels compared to the plasmid control strain (37).

Additionally, our analysis pointed out triple interventions which involved ACLDC and ACLS up-regulation but which, overall, were less effective than the double intervention to increase the 2,3-BDO production rate (**Figure 10**). One such intervention includes the simultaneous up-regulation of acetolactate synthase, acetolactate decarboxylase together with acetaldehyde:ferredoxin oxidoreductase (ACAFDOR), with a 1,86-fold increase in 2,3-BDO production with respect to the wild-type condition ($flux_{ACLDC\ up, ACLS\ up, ACAFDOR\ up}^{2,3-BDO} = 0.070 \pm 0.029$). This latter enzyme, reducing undissociated acetic acid to acetaldehyde, plays a significant role for energy generation, reconstitution of oxidized ferredoxin needed in the Wood-Ljungdahl pathway, and regulation of intracellular acetate levels. According to the kinetic ensemble model used, the acetaldehyde overproduction resulting from the acetaldehyde:ferredoxin oxidoreductase up-regulation could be converted back to acetyl-CoA by the bifunctional aldehyde/alcohol dehydrogenase (NADPH-dependent ACALDy). Several lines of evidence actually suggest that the reaction catalyzed by this latter enzyme does not operate predominantly in the ethanol production direction (41, 42, 48). The Gibbs free energy estimations of the study developing the ensemble kinetic model used here (42) validated the possibility for the reaction to run in reverse (**Figure 2**). Furthermore, the thermodynamics-based metabolic flux analysis of syngas chemostat cultures of *C. autoethanogenum* in ref. 41 showed that the reaction catalyzed by the bifunctional aldehyde/alcohol dehydrogenase is thermodynamically prevented from operating towards ethanol formation. Furthermore, the knockout of the genes encoding the bifunctional aldehyde/alcohol dehydrogenase was found to result in growth reduction and increase in ethanol production (48). Therefore, it is plausible to hypothesize that the acetaldehyde:ferredoxin oxidoreductase, whose up-regulation has been suggested in our analysis, could form an ATP-generating loop, together with the bifunctional aldehyde/alcohol

dehydrogenase operating towards acetyl-CoA, the phosphate acetyltransferase and the acetate kinase.

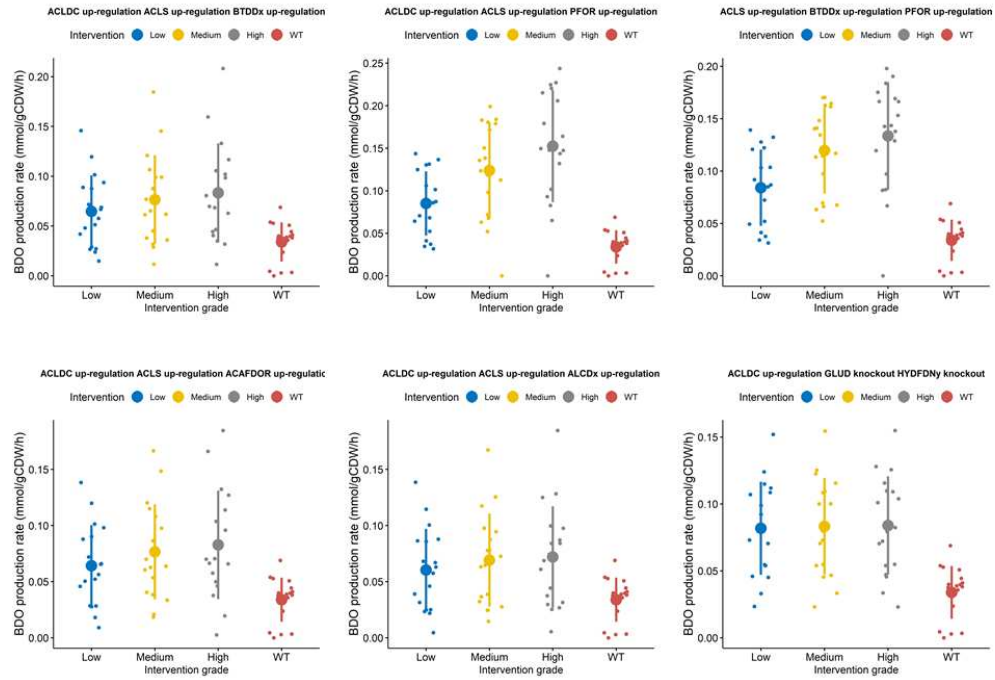


Figure 10. Plots showing the distribution of 2,3-BDO production rates across 18 kinetic parametric sets, under the wild-type scenario and under the triple modification scenario. For each gene involved in a triple intervention, three (low, medium and high) fold changes were simulated. Overlaid are the mean and standard deviation of the 2,3-BDO production rates corresponding to each intervention at each simulated change in gene expression. The figure only refers to selected triple interventions reported in **Table 4**.

Table 4. Summary of third order interventions validated by the kinetic model of *C. autoethanogenum*. Shown are the triple interventions which result in a statistically significant higher 2,3-BDO production rate compared to the WT (Wilcoxon' test, significance level at 1%).

1st reaction	1st intervention	2nd reaction	2nd intervention	3rd reaction	3rd intervention	Adjusted P-value		
						Low	Medium	High

ACLS		BTDDx		PFOR				
$2 \text{ pyr} + \text{h} \rightleftharpoons \text{co2} + \text{acltt}$	up-regulation	$\text{nad} + \text{bdoh} \rightleftharpoons \text{nadh} + \text{h} + \text{actn}$	up-regulation	$\text{coa} + \text{pyr} + \text{Fd}_o\text{x} \rightleftharpoons \text{co2} + \text{accoa} + \text{h} + \text{Fd}_r\text{ed}$	up-regulation	1,91E-04	3,81E-05	3,81E-05
ACLDC		ACLS		PFOR				
$\text{h} + \text{acltt} \rightleftharpoons \text{co2} + \text{actn}$	up-regulation	$2 \text{ pyr} + \text{h} \rightleftharpoons \text{co2} + \text{acltt}$	up-regulation	$\text{coa} + \text{pyr} + \text{Fd}_o\text{x} \rightleftharpoons \text{co2} + \text{accoa} + \text{h} + \text{Fd}_r\text{ed}$	up-regulation	1,91E-04	1,91E-04	3,81E-05
ACLDC		GLUD		HYDFDNY				
$\text{h} + \text{acltt} \rightleftharpoons \text{co2} + \text{actn}$	up-regulation	$\text{h2o} + \text{nadp} + \text{glu-L} \rightleftharpoons \text{nadph} + \text{nh3} + \text{akg} + \text{h}$	knock-out	$\text{nadp} + \text{Fd}_o\text{x} + 2 \text{h2} \rightleftharpoons \text{nadp} + \text{h} + 3 \text{h} + \text{Fd}_r\text{ed}$	knock-out	3,81E-05	1,91E-04	3,81E-05

ACLDC	ACLS		BTD Dx					
$h + alc_{tt} \rightleftharpoons co_2 + actn$	up-regulation	$2 pyr + h \rightleftharpoons co_2 + a_{cltt}$	up-regulation	$nad + bdoh \rightleftharpoons nadh + h + actn$	up-regulation	7,25E-04	7,25E-04	7,63E-05
ACLDC	ACLS		ACA FDO R					
$h + alc_{tt} \rightleftharpoons co_2 + actn$	up-regulation	$2 pyr + h \rightleftharpoons co_2 + a_{cltt}$	up-regulation	$ac + 3 h + Fd_{red} \rightleftharpoons h_2o + acald + Fd_{ox}$	up-regulation	7,25E-04	7,25E-04	7,63E-05
ACLS	FDH		EX_t hf					
$2 pyr + h \rightleftharpoons co_2 + a_{cltt}$	up-regulation	$nadph + 2 co_2 + h + Fd_{red} \rightleftharpoons nadp + 2 for + Fd_{ox}$	knock-out	$thf \rightarrow$	knock-out	7,25E-04	7,25E-04	1,91E-04
ACLDC	ACLS		ALC Dx					
$h + alc_{tt} \rightleftharpoons co_2 + actn$	up-regulation	$2 pyr + h \rightleftharpoons co_2 + a_{cltt}$	up-regulation	$nadh + h + acald \rightleftharpoons nad + etoh$	up-regulation	1,26E-03	1,26E-03	2,67E-04
ACLDC	ACLS		PTA					
$h + alc_{tt} \rightleftharpoons$	up-regulation	$2 pyr + h \rightleftharpoons co_2 + a_{cltt}$	up-regulation	$pi + accoa$	up-regulation	2,67E-03	6,45E-03	3,36E-03

<i>co2 +</i>				<i>+ h</i>				
<i>actn</i>				<i><=></i>				
				<i>coa +</i>				
				<i>actp</i>				
ACLDC		ACLS		RNF				
				<i>nad +</i>				
				<i>3 h +</i>				
				<i>Fd_re</i>				
<i>h + alctt</i>	up-			<i>d</i>	up-	2,00E	2,00E-02	6,45E
<i><=></i>	regulat	<i>2 pyr + h <=></i>	up-	<i><=></i>	regul	-02		-03
<i>co2 +</i>	ion	<i>co2 + acltt</i>	regulation	<i>nadh</i>	ation			
<i>actn</i>				<i>+ 2</i>				
				<i>h_ext</i>				
				<i>+</i>				
				<i>Fd_o</i>				
				<i>x</i>				
ACLDC		ACLS		ACK				
				<i>adp +</i>				
<i>h + alctt</i>	up-			<i>actp</i>	up-	6,45E	2,67E-03	5,20E
<i><=></i>	regulat	<i>2 pyr + h <=></i>	up-	<i><=></i>	regul	-03		-02
<i>co2 +</i>	ion	<i>co2 + acltt</i>	regulation	<i>atp +</i>	ation			
<i>actn</i>				<i>ac +</i>				
				<i>h</i>				

Combining the up-regulation of ACLDC and ACLS with the upregulation of either phosphate acetyltransferase (PTA) or ferredoxin:NAD oxidoreductase (RNF) or acetate kinase (ACK) afforded only lower 2,3-BDO production rate compared to the double intervention encompassing the combined upregulation of ACLDC and ACLS ($flux_{ACLDC\ up, ACLS\ up, PTA\ up}^{2,3-BDO} = 0.050 \pm 0.026$; $flux_{ACLDC\ up, ACLS\ up, RNF\ up}^{2,3-BDO} = 0.056 \pm 0.026$; $flux_{ACLDC\ up, ACLS\ up, ACK\ up}^{2,3-BDO} = 0.067 \pm 0.038$).

A triple intervention leading to a 2-fold increase in 2,3-BDO production rate with respect to the wild-type case ($flux_{ACLDC\ up, GLUD\ KO, HYDFDNY\ KO}^{2,3-BDO} = 0.081 \pm 0.029$) consisted in the ACLDC up-regulation combined with the knockout of glutamate dehydrogenase (GLUD) and the knockout of the electron-bifurcating, NADP- and ferredoxin-dependent [FeFe]-hydrogenase (HYDFDNY), which catalyzes the reversible reduction of NADP and oxidized ferredoxin with 2 H₂ (**Figure 11**). As regards the suggested hydrogenase knockout, it has to be noted that, in addition to the NADP-specific electron-bifurcating [FeFe]-hydrogenase, which is predominantly active on CO (16), the genome of *C. autoethanogenum* harbors also an NADH-dependent electron-bifurcating [Fe-Fe]-hydrogenase reaction, catalyzed by CAETHG_1576-78, which is reflected in the metabolic network used (15). The disruption of the NADP- and ferredoxin-dependent [FeFe]-hydrogenase severely impaired *C. autoethanogenum* growth on a CO-rich gas mix (49). However, this effect was not observable when *C. autoethanogenum* was grown on a H₂-rich gas mix since the disruption of the NADP- and ferredoxin-dependent [FeFe]-hydrogenase was compensated by the expression of other hydrogenases (49). Several lines of evidence suggest that the compensatory role is enacted by the NADH-dependent electron-bifurcating [Fe-Fe]-hydrogenase. Indeed, the inactivation of this hydrogenase caused the microorganism to grow poorly under the H₂-rich condition (49). Moreover, transcriptomic data of a steady state culture of *C. autoethanogenum*, grown on a H₂-rich gas mix over 23 days, showed that the expression of the NADH-dependent electron-bifurcating [Fe-Fe]-hydrogenase increased progressively to reach similar levels of expression as the NADPH-dependent electron-bifurcating [Fe-Fe]-hydrogenase (49). Interestingly, the expression of this hydrogenase did not change in *C. autoethanogenum* fermenting a CO-rich gas mix (23). The increased expression in the H₂-rich condition suggests that the NADH-dependent electron-bifurcating [Fe-Fe]-

hydrogenase plays a critical role in H₂ uptake. Notably, the mutant with inactivated NADP- and ferredoxin-dependent [FeFe]-hydrogenase produced greater amounts of reduced by-products, such as ethanol, compared to the wild-type strain under the H₂-rich condition (49).

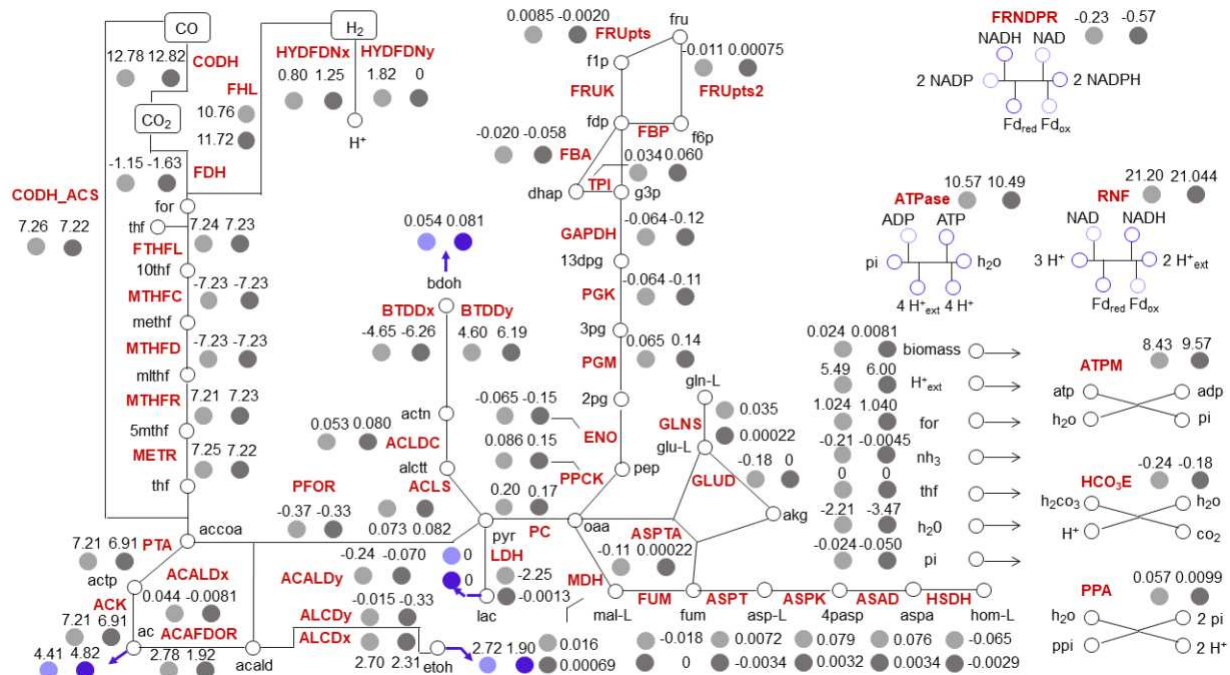


Figure 11. Inferred changes in metabolic fluxes upon the intervention consisting of the acetolactate decarboxylase up-regulation combined with the knockout of glutamate dehydrogenase and the knockout of the electron-bifurcating, NADP- and ferredoxin-dependent [FeFe]-hydrogenase. The map shows simulated fluxes for the reactions in the metabolic network representative of the core metabolism of *C. autoethanogenum* corresponding to the wild-type case (light grey) or to the triple intervention consisting of ACLDC up-regulation, GLUD knockout and HYDFDNy knockout (dark grey). Bolded arrows denote by-products' exchange reactions. Reactions along with enzymes' and metabolites' abbreviations are described in **Supplementary File 1**.

The reduction of acetoin to 2,3-BDO can be carried out by a butanediol dehydrogenase (CAETHG_0385) whose activity has been shown to be favored by NADH (5). Therefore, it is plausible that the reducing equivalents generated by the NAD- and ferredoxin-dependent [FeFe]-hydrogenase, which was shown able to compensate the disruption of the NADP- and ferredoxin-

dependent [FeFe]-hydrogenase in a H₂-rich gas mix, could be used by the NADH-dependent butanediol dehydrogenase to fix carbon into 2,3-BDO.

Finally, the primary-secondary NADPH-alcohol dehydrogenase, which is encoded by CAETHG_0553 in *C. autoethanogenum*, has been shown to be involved in ethanol (18) and 2,3-BDO (16-17) synthesis. Therefore, it is conceivable that the knockout of the NADPH-dependent glutamate dehydrogenase, foreseen in the triple intervention, could increase the availability of reducing equivalents for the 2,3-BDO synthesis by the primary-secondary NADPH-alcohol dehydrogenase.

Overall, our analysis allowed us to identify and comparatively assess the effect on 2,3-BDO production rate of a wide range of single, double and triple interventions. Intuitive and experimentally pursued metabolic engineering strategies, namely the single pyruvate oxidoreductase overexpression or the combined overexpression of pyruvate oxidoreductase with the downstream acetolactate synthase and acetolactate decarboxylase enzymes, were reliably recapitulated (46).

Interestingly, our analysis could prioritize single, double and triple interventions by the relative increase ensured in 2,3-BDO production rate. For instance, our analysis, thanks to the integrated usage of Optforce and kinetic modelling, identified PFOR as the bottleneck reaction in the pathway leading from acetyl-CoA to 2,3-BDO. Indeed, only the combined up-regulation of PFOR with ACLS, among the double interventions, and the combined up-regulation of PFOR with ACLS and ACLDC, among the triple interventions, conferred an increment in 2,3-BDO production rate compared to the PFOR up-regulation alone.

It is worth noting that according to our analysis, interventions partially impinging on by-products branching from acetyl-CoA and pyruvate (acetate, ethanol, amino acids) offer valuable alternatives to the interventions focusing directly on the specific branch from pyruvate to 2,3-BDO. Among the alternative options, the ACK down-regulation, the double interventions combining ACLS up-regulation with glutamate dehydrogenase or ethanol:NAD oxidoreductase knockout and the triple intervention consisting of the ALCDC up-regulation with the knockouts of glutamate dehydrogenase and electron-bifurcating, NADP- and ferredoxin-dependent [FeFe]-hydrogenase, are worthy of attention and further exploration.

Materials and Methods

Genome-scale stoichiometric metabolic model. A couple of GENome-scale Metabolic models (GEMs) are publicly available for *C. autoethanogenum*. The *C. autoethanogenum* GEM iCLAU786 was realized in ref. 23 and refined in ref. 24. The *C. autoethanogenum* GEM Metaclau was made available in ref. 25. iCLAU786 contains 1094 metabolites, 1108 reactions and 643 genes, whereas Metaclau contains 855 metabolites, 849 reactions and 532 genes. Prior to using GEMs for *in silico* design of strains overproducing 2,3-BDO, we validated each GEM by running three tests. We assessed i) the flux through the network in the absence of flux through the exchange reactions, ii) the flux through the non-growth associated ATP hydrolysis reaction in the absence of flux through the uptake reactions. Finally, we benchmarked condition-specific models against several experimental datasets. Step-by-step benchmarking of both models is provided in Validation.m MATLAB script in the GitHub Repository(https://github.com/chan-csu/OptForce_Bdoh/blob/master/Report/Model_Validation/Validation.m) for this project.

Flux through the network with zero exchanges. Exchange reactions were found in iCLAU786 and Metaclau, fluxes through exchange reactions were set to zero and, the sum of absolute flux through the whole network was maximized.

Flux through ATP hydrolysis reaction with zero uptakes. Uptake reactions were found in iCLAU786 and Metaclau, fluxes through exchange reactions were set to zero and the ATP hydrolysis flux was maximized (50).

Condition-specific model validation. The Flux Variability Analysis (FVA) technique uses two linear optimization problems for each reaction of a genomic-scale metabolic reconstruction to evaluate the minimum and maximum values of each reaction rate satisfying the constraints, which occur as inequalities imposing bounds on the system and as mass balance equations imposing mass conservation at steady state. Results obtained through the application of FVA provide insight into the capabilities of a metabolic network to investigate the steady-state behavior of a microorganism. Before applying the model for *in silico* design of strains with potentially superior characteristics, it is advisable to assess the accuracy of the model by constraining the GEM with publicly available experimental data. More precisely, we constrained the GEM with substrate uptake rates, maximized biomass yield in FVA calculations, and compared model predictions with published experimental data concerning specific growth rate and by-products' production rates. We surveyed the literature stored at Web of Science Core Collection, PubMed and individual publisher websites for research articles focused on CO-based gas fermentations with *C. autoethanogenum* and reporting quantitative data on gas exchange rates as well as biomass and by-products' formation rates (**Table 1**). FVA as a means of model validation was run using scripts in the Cobra Toolbox v.3.0 (40) and Gurobi Optimizer version 9.1 (<https://www.gurobi.com/products/gurobi-optimizer/>) as the optimization solver. The GEM

was constrained with experimentally quantitated gas uptake rates. The objective used in the simulations was maximizing the biomass formation rate. Finally, the experimentally reported values for acetate, ethanol, 2,3-BDO and biomass formation rate were contrasted with the range of allowed values resulting from FVA. Furthermore, Flux Balance Analysis (FBA) was used to predict acetate, ethanol, 2,3-BDO and biomass formation rate corresponding to each dataset included in **Table 1** and to assess the consistency of FBA predicted values with the experimental values reported in **Table 1**. The files containing the experimental data obtained by literature mining, the iCLUA786 and Metaclau GEMs and the script used for model validation are available in the GitHub Repository (https://github.com/chan-csu/OptForce_Bdoh/tree/master/Report/Model_Validation).

Relationship between gas feeding and CO₂ production. We varied the fluxes through CO and H₂ uptake reactions step-wise in the range [0 mmol/g_{CDW}/h; -50 mmol/g_{CDW}/h] and the optimal objective value was calculated as a function of those fluxes. We investigated the effects of varying gaseous substrates' uptake rates on 2,3-BDO production rate and CO₂ production rate.

Prediction of interventions enhancing 2,3-butanediol production. The genome-scale metabolic reconstruction Metaclau was constrained with CO and H₂ uptake rates set to 20 and 33 mmol/g_{CDW}/h, which we retrieved from the gas fermentation study described in ref. 38. The model was used to simulate the *in silico* design and screening of strains with gene modifications which, subject to the model stoichiometry and boundary conditions, could lead to the production of higher yields of the 2,3-BDO compound. The design and screening of mutant strains were carried out using the computational tool Optforce (39) as it is implemented in the Cobra Toolbox v.3.0 within the Matlab environment. In the first step, biomass exchange reaction was set as the

objective function to find the maximum attainable growth rate, and this assumed to present the wild type strain. Maximum attainable growth rate was multiplied by 0.1 to obtain a lower bound on growth to ensure that the organism can grow in all of the suggested interventions. In the next step Optforce with 2,3-BDO exchange as objective was used to find 2,3-BDO maximizing phenotype. OptForce compares the flux ranges between the wildtype and butanediol maximizing mutant using flux variability analysis to suggest interventions

(https://raw.githubusercontent.com/chan-csu/OptForce_Bdoh/master/Final_Script.m). The perturbations suggested by Optforce to meet the overproduction target can include the increase or decrease in the flux values of particular reactions or the elimination of particular reaction fluxes, which can be achievable through genes' over-expression, down-regulation or knockout, respectively. In particular, the top 500 theoretical interventions (first, second, and third order interventions), which were found consistent with the imposed 2,3-BDO overproduction target according to the Optforce strain design procedure, were retained for further independent validation.

Simulations using the kinetic model of *C. autoethanogenum*

Interventions were further analyzed through a kinetic model of the *C. autoethanogenum* core metabolism previously developed with the Ensemble Modeling framework (42). The kinetic model accounts for 70 reactions and 62 metabolites. Briefly, in the ensemble modeling framework, every reaction in the network was decomposed as elementary reactions with elementary kinetics. Using the Gibbs free energy and range for internal metabolite concentrations as constraints, a large number of thermodynamically feasible kinetic parameter sets were randomly sampled and screened for the convergence and fitness to three sets of experimental growth data for *C. autoethanogenum* in ref. 42, finally resulting in an ensemble of

18 kinetic parameter sets that were used in this work to validate Optforce predictions. The validation of Optforce predictions by kinetic modeling was restricted to the subset of reactions encompassed by both methods. **Supplementary File 1** provides the lists of reactions and metabolites included in the metabolic reconstruction (https://github.com/chan-csu/OptForce_Bdoh/raw/master/Results/Supplementary_File1.xlsx). The kinetic ensemble model of *C. autoethanogenum* was employed to calculate the change in 2,3-BDO production rate as a function of changing enzymes' expression levels according to the combinations of single, double and triple interventions on reactions fluxes, which were suggested by Optforce. We set three fold change (FC) values in enzymes' expression: FC = 1.1, 1.3 and 1.5 for up-regulation and FC = 0.9, 0.7 and 0.5 for down-regulation. The kinetic representation of the core metabolism was constrained by a single reference state where the CO and H₂ uptake rates were set to 20 and 33 mmol/g_{CDW}/h, respectively. By calculating the forward finite difference slopes for each intervention across each of the final 18 kinetic parameter sets, we obtained a distribution of 2,3-BDO production rates in correspondence to each intervention. In order to identify the interventions that reflect in a statistically significant higher production of 2,3-BDO compared to the wild-type strain, we applied the pairwise Wilcoxon's test. Raw P-values were adjusted for multiple testing by the Bonferroni approach. Statistical analysis was performed within the R software environment for statistical computing.

References

1. Bae J, Song Y, Lee H, Shin J, Jin S, Kang S, Cho BK. 2022. Valorization of C1 gases to value-added chemicals using acetogenic biocatalysts. *Chem Eng J* 428:131325 doi: [10.1016/j.cej.2021.131325](https://doi.org/10.1016/j.cej.2021.131325).
2. Fackler N, Björn D, Heijstra BD, Rasor BJ, Brown H, Martin J, Ni Z, Shebek KM, Rosin RR, Simpson SD,¹ Tyo KE, Giannone RJ, Hettich RL, Tschaplinski TJ, Leang C, Brown SD, Jewett MC, Köpke M. 2021. Stepping on the Gas to a Circular Economy: Accelerating Development of Carbon-Negative Chemical Production from Gas Fermentation. *Annu Rev Chem Biomol E* 7(12):439-470.
3. Jack J, Lo J, Maness PC, Ren ZJ. 2019. Directing *Clostridium ljungdahlii* fermentation products via hydrogen to carbon monoxide ratio in syngas. *Biomass Bioenergy* 124:95-101.
4. [Ragsdale](#) SW, [Pierce](#) E. 2008. Acetogenesis and the Wood-Ljungdahl pathway of CO(2) fixation. *Biochim Biophys Acta* 1784(12):1873-98.
5. [Köpke](#) M, [Mihalcea](#) C, [Liew](#) F, [Tizard](#) JH, [Ali](#) MS, [Conolly](#) JJ, [Al-Sinawi](#) B, [Simpson](#) SD. 2011. 2,3-butanediol production by acetogenic bacteria, an alternative route to chemical synthesis, using industrial waste gas. *Appl Environ Microbiol* 77(15):5467-75.
6. [Bengelsdorf](#) FR, [Poehlein](#) A, [Linder](#) S, [Erz](#) C, [Hummel](#) T, [Hoffmeister](#) S, [Daniel](#) R, [Dürre](#) P. 2016. Industrial Acetogenic Biocatalysts: A Comparative Metabolic and Genomic Analysis *Front Microbiol* 7:1036 doi:[10.3389/fmicb.2016.01036](https://doi.org/10.3389/fmicb.2016.01036).
7. Lee J, Lee JW, Chae CG, Kwon SJ, Kim YJ, Lee JH, Lee HS. 2019. Domestication of the novel alcohologenic acetogen *Clostridium* sp. AWRP: from isolation to characterization for syngas fermentation. *Biotechnol Biofuels* 12:228 doi:10.1186/s13068-019-1570-0.
8. [Song](#) CW, [Park](#) JM, [Chung](#) SC, Lee SY, [Song](#) H. 2019. Microbial production of 2,3-butanediol for industrial applications. *J Ind Microbiol Biotechnol* 46(11):1583-1601.
9. Huynh TT, Le MD, Duong DN. 2019. Effects of butanol–gasoline blends on SI engine performance, fuel consumption, and emission characteristics at partial engine speeds. *Int J Energy Environ Eng* 10:483–492.
10. Knowlton JW, Schieltz NC, Macmillan D. 1946. Physical chemical properties of the 2,3-butanediols. *J. Am. Chem. Soc.* 68:208-210.
11. [Celińska](#) E, [Grajek](#) W. 2009. Biotechnological production of 2,3-butanediol--current state and prospects. *Biotechnol Adv.* 27(6):715-725.
12. [Paciorek-Sadowska](#) J, Czupryński B. 2006. New compounds for production of polyurethane foams. *Journal of Applied Polymer Science* 102(6):5918-5926.

13. [Baek](#) HS, Woo BY, Yoo SJ, Joo YH, Shin SS, Oh MH, Lee JH, Kim SY. Januray 2020. Composition containing meso-2,3-butanediol. US10525017B2.
14. Brown, SD, Nagaraju S, Utturkar S, De Tissera S, Segovia S, Mitchell W, Land ML, Dassanayake A, Köpke M. 2014. Comparison of single-molecule sequencing and hybrid approaches for finishing the genome of *Clostridium autoethanogenum* and analysis of CRISPR systems in industrial relevant Clostridia. *Biotechnol. Biofuels* 7:40 doi:10.1186/1754-6834-7-40.
15. Mock J, Zheng Y, Mueller AP, Ly S, Tran L, Segovia S, [Nagaraju](#) S, [Köpke](#) M, [Dürre](#) P, [Thauer](#) RK. 2015. Energy conservation associated with ethanol formation from H₂ and CO₂ in *Clostridium autoethanogenum* involving electron bifurcation. *J. Bacteriol.* 197:2965–2980.
16. [Wang](#) S, [Huang](#) H, [Kahnt](#) J, [Mueller](#) AP, [Köpke](#) M, [Thauer](#) RK. 2013. NADP-specific electron-bifurcating [FeFe]-hydrogenase in a functional complex with formate dehydrogenase in *Clostridium autoethanogenum* grown on CO. *J Bacteriol.* 195(19):4373-86.
17. Köpke M, Gerth ML, Maddock DJ, Mueller AP, Liew F, Simpson SD, [Patrick](#) WM. 2014. Reconstruction of an acetogenic 2,3-butanediol pathway involving a novel NADPH-dependent primary-secondary alcohol dehydrogenase. *Appl. Environ. Microbiol.* 80:3394–3403.
18. Richter H, Molitor B, Wei H, Chen W, Aristilde L, Angenent LT. 2016. Ethanol production in syngas-fermenting *Clostridium ljungdahlii* is controlled by thermodynamics rather than by enzyme expression. *Energy Environ. Sci.* 9:2392-2399.
19. Simpson SD, [Shane E. Fleming](#) SE, Havill AM, RTrevethick S. February 2012. Process for producing chemicals using microbial fermentation of substrates comprising carbon monoxide. WO2012024522A3.
20. Simpson SD, Collet C, Mihalcea CD, Conolly JJ, Waters GW. October 2012. A fermentation process for controlling butanediol production. WO2012131627.
21. Smart KF, Mueller AP, Mawdsley MJH, Mihalcea CD. March 2015. A fermentation process. WO2015042550.
22. Smart KF, Ly BS. November 2015. Fermentation process for the production and control of pyruvate-derived products. WO2015179578.
23. Esteban M, Behrendorff JB, Nagaraju S, DeTissera S, Segovia S, Palfreyman RW, Daniell J, Licon-Cassani C, Quek L, Speight R, Hodson MP, Simpson SD, Mitchell WP, Köpke M, Nielsen LK. 2016. Low carbon fuels and commodity chemicals from waste gases – systematic approach to understand energy metabolism in a model acetogen. *Green Chem* 18:3020-3028.

24. Valgepea K, Loi KQ, Behrendorff JB, Lemgruber RSP, Plan M, Hodson MP, Köpke M, Nielsen LK, Marcellin E. 2017. Arginine deiminase pathway provides ATP and boosts growth of the gas-fermenting acetogen *Clostridium autoethanogenum*. *Metab Eng.* 41:202-211.
25. [Norman](#) ROJ, [Millat](#) T, [Schatschneider](#) S, [Henstra](#) AM, [Breitkopf](#) R, [Pander](#) B, [Annan](#) FJ, [Piatek](#) P, [Hartman](#) HB, [Poolman](#) MG, [Fell](#) DA, [Winzer](#) K, Nigel NP, [Hodgman](#) C. 2019. Genome-scale model of *C. autoethanogenum* reveals optimal bioprocess conditions for high-value chemical production from carbon monoxide. *Engineering Biology* 3(2):32-40.
26. Bordbar A, Monk JM, King ZA, Palsson BØ. 2014. Constraint-based models predict metabolic and associated cellular functions. *Nat Rev Genet* 15(2):107-20.
27. Jeffrey D Orth JD, Thiele I & Palsson BØ. 2010. What is flux balance analysis? *Nat Biotechnol* 28: 245–248.
28. Strutz J, Martin J, Greene J, Broadbelt L, Tyo K. 2019. Metabolic kinetic modeling provides insight into complex biological questions, but hurdles remain. *Curr Opin Biotechnol.* 59:24-30.
29. Tran LM, Rizk ML, Liao JC. 2008. Ensemble Modeling of Metabolic Networks. *Biophysical Journal* 95 (12): 5606-5617.
30. Lee Y, Lafontaine Rivera JG, Liao JC. 2014. Ensemble Modeling for Robustness Analysis in engineering non-native metabolic pathways. *Metab Eng.* 25:63-71.
31. Wu C, Jiang H, Kalra I, Wang X, Cano M, Maness P, Yu J, Xiong W. 2020. A Generalized Computational Framework to Streamline Thermodynamics and Kinetics Analysis of Metabolic Pathways. *Metab Eng.* 57: 140-150.
32. Schuchmann K, Muller V. 2014. Autotrophy at the thermodynamic limit of life: a model for energy conservation in acetogenic bacteria. *Nat Rev Microbiol.* 12(12):809-21.
33. Bengelsdorf FR, Beck MH, Erz C, Hoffmeister S, Karl MM, Riegler P, et al. 2018. Bacterial anaerobic synthesis gas (syngas) and CO₂ + H₂ fermentation. *Adv. Appl. Microbiol.* 103: 143–221.
34. Tremblay PL, Zhang T, Dar SA, Leang C, Lovley DR. 2012. The Rnf complex of *Clostridium ljungdahlii* is a proton-translocating ferredoxin:NAD⁺ oxidoreductase essential for autotrophic growth. *mBio* 4(1): e00406-12.
35. Wilkins MR, Atiyeh HK. 2011. Microbial production of ethanol from carbon monoxide. *Curr Opin Biotechnol.* 22(3):326-3010.
36. Molitor B, Richter H, Martin ME, Jensen RO, Juminaga A, Mihalcea C, Angenent LT. 2016. Carbon recovery by fermentation of CO-rich off gases - Turning steel mills into biorefineries. *Bioresour Technol.* 215:386-396.

37. Bertsch J, Müller V. 2015. Bioenergetic constraints for conversion of syngas to biofuels in acetogenic bacteria. *Biotechnol Biofuels* 8:210 doi:10.1186/s13068-015-0393-x.
38. Valgepea K, Lemgruber RSP, Abdalla T, Binos S, Takemori N, Takemori A, Tanaka Y, Tappel R, Köpke M, Simpson SD, Nielsen LK, Marcellin E. 2018. H₂ drives metabolic rearrangements in gas-fermenting *Clostridium autoethanogenum*. *Biotechnol Biofuels* 11:55 doi:10.1186/s13068-018-1052-9
39. Ranganathan S, Suthers PF, Maranas CD. 2010. OptForce: An Optimization Procedure for Identifying All Genetic Manipulations Leading to Targeted Overproductions. *PLoS Comput Biol* 6(4):e1000744 doi: 10.1371/journal.pcbi.1000744.
40. [Heirendt L](#), [Arreckx S](#), [Pfau T](#), [Mendoza SN](#), [Richelle A](#), [Heinken A](#), [Haraldsdóttir HS](#), [Wachowiak J](#), [Keating SM](#), [Vlasov V](#), [Magnusdóttir S](#), [Ng CY](#), [Preciat G](#), [Žagare A](#), [Chan SHJ](#), [Aurich MK](#), [Clancy CM](#), [Modamio J](#), [Sauls JT](#), [Noronha A](#), [Bordbar A](#), [Cousins B](#), [El Assal DC](#), [Valcarcel LV](#), [Apaolaza I](#), [Ghaderi S](#), [Ahookhosh M](#), [Guebila MB](#), [Kostromins A](#), [Sompairac N](#), [Le HM](#), [Ma D](#), [Sun Y](#), [Wang L](#), [Yurkovich JT](#), [Oliveira MAP](#), [Vuong PT](#), [El Assal LP](#), [Kuperstein I](#), [Zinovyev A](#), [Hinton HS](#), [Bryant WA](#), [Aragón Artacho FJ](#), [Planes FJ](#), [Stalidzans E](#), [Maass A](#), [Vempala S](#), [Hucka M](#), [Saunders MA](#), [Maranas CD](#), [Lewis NE](#), [Sauter T](#), [Palsson BØ](#), [Thiele I](#), [Fleming RMT](#). 2019. Creation and analysis of biochemical constraint-based models: the COBRA Toolbox v3.0. *Nat Protoc* 14(3):639–702.
41. Mahamkali V, Valgepea K, Lemgruber RSP, Plan M, Tappel R, Köpke M, Simpson SD, Lars Keld Nielsen LK, Marcellin E. 2020. Redox controls metabolic robustness in the gas-fermenting acetogen *Clostridium autoethanogenum*. *Proc Natl Acad Sci U S A* 117(23):13168-13175.
42. Greene J, Daniell J, [Köpke M](#), Broadbelt L, Tyo KEJ. 2019. Kinetic ensemble model of gas fermenting *Clostridium autoethanogenum* for improved ethanol production. *Biochem Eng J* 148: 46-56.
43. Tran LM, Rizk ML, Liao JC. 2008. Ensemble Modeling of Metabolic Network. *Biophysical J* 95(12):5606-5617.
44. Tan Y, Lafontaine Rivera JG, Contador CA, Asenjo JA, Liao JC. 2011. Reducing the allowable kinetic space by constructing ensemble of dynamic models with the same steady-state flux. *Metab Eng* 13(1):60-75.
45. Valgepea K, Lemgruber RSP, Meaghan K, Palfreyman RW, Abdalla T, Heijstra BD, Behrendorff JB, Ryan Tappel R, Köpke M, Simpson SD, Lars Keld Nielsen LK, Marcellin E. 2017. Maintenance of ATP Homeostasis Triggers Metabolic Shifts in Gas-Fermenting Acetogens. *Cell Syst* 4(5):505-515.e5.
46. Köpke M, Mueller AP. December 2014. Recombinant microorganisms exhibiting increased flux through a fermentation pathway. WO2014197746A1.

47. Katsyv A, Müller V. 2020. Overcoming Energetic Barriers in Acetogenic C1 Conversion. *Front. Bioeng. Biotechnol.* 8:621166 doi:10.3389/fbioe.2020.621166.
48. Liew F, Henstra AM, Köpke M, Winzer K, Simpson SD, Minton NP. 2017. Metabolic engineering of *Clostridium autoethanogenum* for selective alcohol production. *Metab Eng* 40:104-114.
49. Nagaraju S, Köpke M. July 2017. Microorganism with modified hydrogenase activity. WO2017117309A1.
50. Mahadevan R, Schilling CH. 2003. The effects of alternate optimal solutions in constraint-based genome-scale metabolic models. *Metab Eng* 5(4):264-276.

Appendix

Supplementary File 1. The file reports the single, double and triple interventions produced by Optforce. For each intervention, this file provides the reactions involved along with the change proposed (up-regulation, down-regulation, knockout). This spreadsheet can be found in:

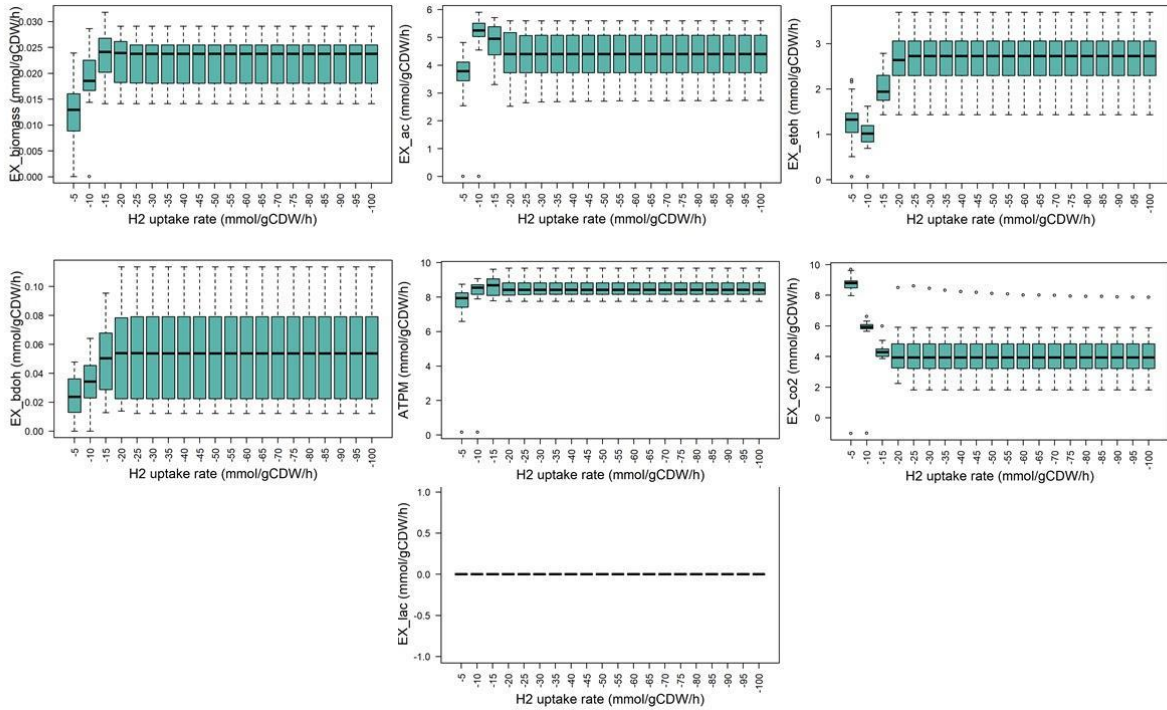
https://github.com/chan-csu/OptForce_Bdoh/raw/master/Results/Supplementary_File1.xlsx

Supplementary File 2. The table reports the reactions and metabolites included in the network representation of *C. autoethanogenum* core metabolism. This spreadsheet can be found in:

https://github.com/chan-csu/OptForce_Bdoh/raw/master/Results/Supplementary_Table_1.xlsx

CO ₂ excretion rate (mmol/gCDW/h)		H ₂ uptake rate (mmol/gCDW/h)										
		0	-5	-10	-15	-20	-25	-30	-35	-40	-45	-50
CO uptake rate (mmol/gCDW/h)	-5	NA	[0.00;1.1]	[0.00;0.082]	NA							
	-10	[4.2;6.6]	[1.1;4.9]	[0.00;3.2]	[0.00;1.7]	[0.00;0.28]	NA	NA	NA	NA	NA	NA
	-15	[5.8;9.9]	[2.7;8.3]	[0.00;6.6]	[0.00;4.9]	[0.00;3.3]	[0.00;1.7]	[0.00;0.47]	[0.00;0.11]	NA	NA	NA
	-20	[7.3;13]	[4.2;12]	[1.1;9.9]	[0.00;8.2]	[0.00;6.5]	[0.00;4.9]	[0.00;3.3]	[0.00;1.7]	[0.00;0.66]	[0.00;0.30]	NA
	-25	[8.9;17]	[5.8;15]	[2.7;13]	[0.00;12]	[0.00;9.8]	[0.008.2]	[0.00;6.6]	[0.00;5.00]	[0.00;3.4]	[0.00;1.8]	[0.00;0.86]
	-30	[10;20]	[7.3;18]	[4.2;17]	[1.1;15]	[0.00;13]	[0.00;11]	[0.00;9.8]	[0.00;8.2]	[0.00;6.6]	[0.00;5.0]	[0.00;3.4]
	-35	[12;23]	[8.9;22]	[5.8;20]	[2.7;18]	[0.00;16]	[0.00;15]	[0.00;13]	[0.00;11]	[0.00;9.8]	[0.00;8.2]	[0.00;6.7]
	-40	[14;27]	[10;25]	[7.3;23]	[4.2;22]	[1.1;20]	[0.00;18]	[0.00;16]	[0.00;15]	[0.00;13]	[0.00;11]	[0.00;9.9]
	-45	[15;30]	[12;28]	[8.9;27]	[5.8;25]	[2.7;23]	[0.00;21]	[0.00;20]	[0.00;18]	[0.00;16]	[0.00;15]	[0.00;13]
-50	[17;33]	[14;32]	[10;30]	[7.3;28]	[4.2;26]	[1.1;25]	[0.00;23]	[0.00;21]	[0.00;20]	[0.00;18]	[0.00;16]	
2,3-BDO excretion rate (mmol/gCDW/h)		H ₂ uptake rate (mmol/gCDW/h)										
		0	-5	-10	-15	-20	-25	-30	-35	-40	-45	-50
CO uptake rate (mmol/gCDW/h)	-5	NA	[0.00;0.089]	[0.00;0.10]	NA							
	-10	[0.00;0.15]	[0.00;0.27]	[0.00;0.39]	[0.00;0.51]	[0.00;0.35]	NA	NA	NA	NA	NA	NA
	-15	[0.00;0.34]	[0.00;0.45]	[0.00;0.57]	[0.00;0.68]	[0.00;0.85]	[0.00;0.93]	[0.00;0.60]	[0.00;0.13]	NA	NA	NA
	-20	[0.00;0.52]	[0.00;0.63]	[0.00;0.75]	[0;0.87]	[0;0.98]	[0;1.2]	[0;1.3]	[0;1.3]	[0;0.84]	[0;0.38]	NA
	-25	[0.00;0.70]	[0.00;0.82]	[0.00;0.93]	[0.00;1.0]	[0.0;1.2]	[0.0;1.3]	[0.0;1.5]	[0.0;1.6]	[0.0;1.7]	[0.0;1.8]	[0.0;1.1]
	-30	[0.00;0.88]	[0.00;1.0]	[0.00;1.1]	[0.00;1.2]	[0.00;1.3]	[0.00;1.5]	[0.00;1.6]	[0.00;1.8]	[0.00;1.9]	[0.00;2.0]	[0.00;2.1]
	-35	[0.00;1.1]	[0.0;1.2]	[0.00;1.3]	[0.00;1.4]	[0.00;1.5]	[0.00;1.6]	[0.00;1.8]	[0.00;1.9]	[0.00;2.1]	[0.00;2.3]	[0.00;2.4]
	-40	[0.00;1.2]	[0.00;1.4]	[0.00;1.5]	[0.00;1.6]	[0.00;1.7]	[0.00;1.8]	[0.00;1.9]	[0.00;2.1]	[0.00;2.2]	[0.00;2.4]	[0.00;2.6]
	-45	[0.00;1.4]	[0.00;1.5]	[0.00;1.7]	[0.00;1.8]	[0.00;1.9]	[0.00;2]	[0.00;2.1]	[0.00;2.2]	[0.00;2.4]	[0.00;2.5]	[0.00;2.7]
-50	[0.00;1.6]	[0.00;1.7]	[0.00;1.8]	[0.00;2.0]	[0.00;2.1]	[0.00;2.2]	[0.00;2.3]	[0.00;2.4]	[0.00;2.5]	[0.00;2.6]	[0.00;2.8]	

Supplementary Figure 1. The Figure shows the 2,3-BDO and CO₂ production rate obtained by performing FVA at varying uptake rates for CO and H₂. Highlighted in blue are the combinations of gas uptake rates that do not produce CO₂.



Supplementary Figure 2. This figure shows the distribution of fluxes across 18 kinetic parametric sets of the exchange reactions for acetate, ethanol, 2,3-butanediol, lactate, CO₂ and biomass as well as of the ATPM reaction at increasing H₂ uptake rates while preserving the CO₂ uptake rate at 20 mmol/gCDW/h.